Available online at www.sciencedirect.com
SCIENCE DIRECT
Coordination Chemistry Reviews 250 (2006) 948–973
COORDINATION CHEMISTRY REVIEWS
www.elsevier.com/locate/ccr

Review

# Optical properties of Cm(III) in crystals and solutions and their application to Cm(III) speciation

Norman M. Edelstein [a,*], Reinhardt Klenze [b], Thomas Fanghänel [b], Solange Hubert [c]

[a] *Chemical Sciences Division, Lawrence Berkeley National Laboratory, Berkeley, CA 94720, USA*
[b] *Institut für Nukleare Entsorgung, Forschungszentrum Karlsruhe, P. O. Box 3640, 76021 Karlsruhe, Germany*
[c] *Institut de Physique Nucléaire, IN2P3 - CNRS, UMR8608, 91406 Orsay, France*

Received 24 July 2005; accepted 7 February 2006
Available online 6 March 2006

## Contents



* Corresponding author. Tel.: +1 510 486 5624; fax: +1 510 486 5596.
*E-mail address:* nmedelstein@lbl.gov (N.M. Edelstein).

0010-8545/$ – see front matter 
doi:10.1016/j.ccr.2006.02.004

**Abstract**

Cm(III), atomic number 96, has the electronic configuration [Rn core, $5f^7$] and is the actinide analog of the lanthanide ion $Gd^{3+}$ [Xe core, $4f^7$]. The ground term has only ~78% $^8S_{7/2}$ parentage due to the large spin–orbit interaction as compared to the almost 100% $^8S_{7/2}$ parentage for $Gd^{3+}$. The electrostatic interaction between equivalent electrons in the $f^7$ shell results in a large gap between the octet state ($^8S_{7/2}$) of the ground term and the sextet states ($^6D_{7/2}$, $^6P_{7/2}$, $^6P_{5/2}$, ...) of the excited multiplets. For $Gd^{3+}$ this splitting results in a gap greater than 30,000 $cm^{-1}$. The greater spatial extent of the 5f electron shell results in a smaller electrostatic interaction between equivalent electrons in the 5f shell than in the 4f shell. Thus for Cm(III), this splitting is on the order of 16,800 $cm^{-1}$. The ground term multiplet splitting is small (~2–50 $cm^{-1}$) because the largest component of the ground multiplet has zero angular momentum. The large gap between the first excited multiplet and the ground term results in strong fluorescence. The lifetime of this fluorescence is sensitive to the number and nature of the ligands in the first coordination shell in solution and solid complexes as is the energy of the transition. From measurements of this lifetime the number of $H_2O$ molecules in this coordination shell can be determined. In this paper the theories necessary to analyze the energy level spectra of the Cm(III) in crystals and Cm(III) solution intensities are briefly discussed. Applications of Cm(III) fluorescence measurements for the determination of solution and solid species are reviewed.


*Keywords:* Cm(III); Optical properties; Fluorescence; Energy levels; Crystals; Speciation; Aquatic system; Trace concentration

## 1. Introduction

Curium is element 96 in the periodic table. The ground electronic configuration of the free atom consists of the radon core plus the $5f^7 6d7s^2$ electrons. The most stable oxidation state is Cm(III), whose ground electronic configuration is [Rn] $5f^7$. Since the full 5f configuration would contain 14 5f electrons, $Cm^{3+}$ has a half-filled 5f shell. The ground term of Cm(III) will have maximum multiplicity from the seven unpaired 5f electrons resulting in an $^8S_{7/2}$ multiplet. The next highest free ion term will contain five unpaired f electrons (spin up) and two paired 5f electrons (one 5f electron with spin up is paired with a second 5f electron with spin down) with a total spin angular momentum of $S = 5/2$. The energy necessary to excite one of the unpaired 5f electrons to the next highest multiplet is quite high due to the stability of the maximum multiplicity state. However, it is less than that needed for its lanthanide counterpart, Gd(III) (atomic number 64, [Xe] $4f^7$) due primarily to the smaller electrostatic (Coulombic) interactions in the actinides. Another factor contributing to the smaller gap between the ground and first excited multiplet in Cm(III) compared to Gd(III), is the larger spin–orbit coupling in the actinide series, which causes larger admixtures of L–S terms with $J = 7/2$ with the ground term [1]. A comparison of the free ion levels for Cm(III) and Gd(III) is shown in Fig. 1. For both ions a large energy gap exits between the ground and first excited states, however, for Cm(III) this gap is ~16,800 $cm^{-1}$ while for Gd(III) the gap is ~32,000 $cm^{-1}$, in the ultra-violet region. The occurrence of the Cm(III) first excited multiplet in the visible region with a large energy gap to the ground term means that fluorescence can readily be observed from the lowest level of this multiplet.

The aquatic chemistry of actinide ions has attracted great attention in the last two decades in order to validate long-term predictions of radionuclide migration in the near and far field of a high level nuclear waste repository. Presently, chemical infor-

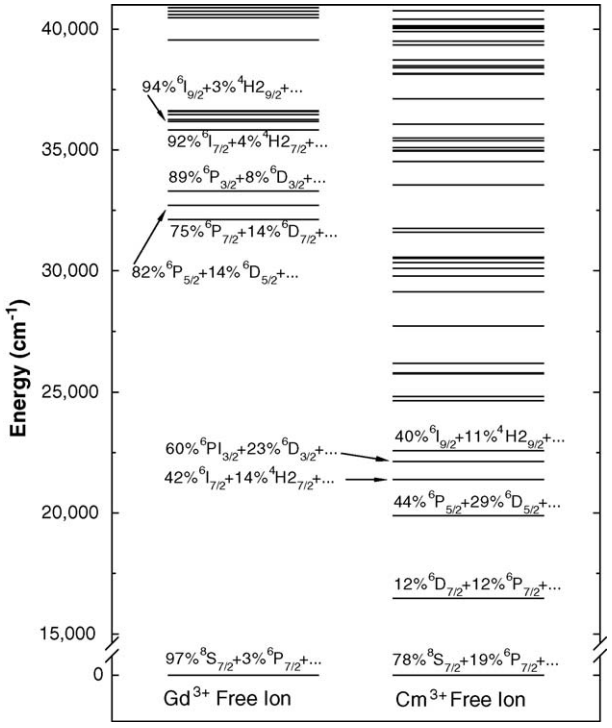


Fig. 1. A comparison of the free ion energy levels and wavefunctions of the $Gd^{3+}$ and $Cm^{3+}$ ions.

mation on the migration behavior of radionuclides for safety studies comes from empirical site-specific sorption parameters and solubilities. However, reliable long-term predictions cannot depend on empirical parameters but must be based on sound scientific principles such as the laws of thermodynamics. An understanding of the ongoing processes at a molecular level, e.g. the coordination chemistry of actinide ions, is necessary for a full thermodynamic description.

The solubility of the highly charged actinide ions in natural groundwaters is sparingly low (usually $<10^{-6}$ M). In addition, the various actinide species are usually in fast equilibrium, thus analytical detection after fractionation of the species is not applicable. Common speciation tools such as XAFS, NMR or conventional optical spectroscopy lack the requested sensitivity. Beitz and Hessler proposed the use of laser-based methods, such as laser-induced photothermal absorption and time-resolved laser fluorescence spectroscopy (TRLFS) of the 5f-transitions [2]. The latter method proved to be highly sensitive and selective for the speciation of Cm(III) in aqueous and non-aqueous solutions, at the mineral/water interface, or incorporated into the bulk mineral phase. As will be demonstrated later in this review, TRLFS on Cm(III) has the potential to provide useful speciation and structural information at relevant trace level concentrations, which are not assessable by any other method for any other metal ion, e.g. Fe, within the periodic table. Another field of application is the separation chemistry of actinides, especially the separation of trivalent actinides from lanthanides by solvent extraction with respect to partitioning and transmutation of minor actinides. Compared to the spectroscopy on Eu(III) and Tb(III), which has been applied recently in various fields of material and life sciences, the application of Cm(III) TRLFS as a speciation method is still in its infancy.

This review will cover the fundamental electronic structure and spectroscopy of the Cm(III) ion in crystals and then describe how the fluorescence spectra and fluorescence lifetimes of the Cm(III) in solutions or on surfaces can be utilized to obtain information about the coordination geometry. Although only a small number of groups are working worldwide in this field, this review will not cover all published results but will focus on a few notable examples that illustrate the potential and limitations of this method. The review will be confined mainly to coordination chemistry results; the thermodynamic aspects will be described only briefly.

## 2. Theory

### 2.1. Energy levels – crystal field parameters

The observed energy levels are fitted to a phenomenological Hamiltonian $H = H_{FI} + H_{CF}$ by a simultaneous diagonalization of the free ion Hamiltonian $H_{FI}$ and the crystal field Hamiltonian $H_{CF}$. The free ion Hamiltonian is given as follows:

$$H_{FI} = \sum_{k=0,2,4,6} F^k(\mathrm{nf,\,nf})\, f_k + \zeta_f \alpha_{S.O.} + \alpha L(L+1) + \beta G(G_2) + \gamma G(R_7) + \sum_{\substack{k=2-8 \\ k\neq 5}} T^k t_k + \sum_{k=0,2,4} M^k m_k + \sum_{k=2,4,6} P^k p_k, \quad (1)$$

where $F^k$(nf, nf)'s and $\zeta_f$ represent the radial parts of the electrostatic and spin–orbit interaction, respectively, between f electrons, and $f_k$ and $\alpha_{S.O.}$ are the angular parts of these interactions. The parameters, $\alpha$, $\beta$ and $\gamma$, are associated with the two-body effective operators of the configuration interaction and the $T^k$'s are the corresponding parameters for the three-body-configuration interaction. The $M^k$ parameters arise from spin–spin and spin-other-orbit interactions and the $P^k$ parameters represent the electrostatic–spin–orbit interaction with higher configurations. The $T^k$, $M^k$ and $P^k$ are the radial parts of the interactions, whereas $t_k$, $m_k$ and $p_k$ are the corresponding angular parts. For the different interactions the angular parts can be evaluated exactly; the radial parts are treated as parameters [3,4].

The crystal field Hamiltonian is expressed in terms of the phenomenological crystal field parameters $B_q^k$ and the angular tensor operators $C_q^k$ as follows:

$$H_{CF} = \sum_{k,q,i} B_q^k (C_q^k)_i \quad (2)$$

where the sum involving $i$ is over all the f electrons. The values of $k$ and $q$ are limited by the point symmetry of the $f^N$ ion site. For states of the same parity, $k$ will have only even values. The term for which $k=0$ and $q=0$ shifts all levels of an $f^N$ configuration equally and is not utilized in fitting levels within one configuration [5].

The quality of fits to the above expressions was determined using the deviation $\sigma$ (in $\mathrm{cm}^{-1}$), which is defined as:

$$\sigma = \sum \left[ \frac{(E_{exp} - E_{calc})^2}{(n-p)} \right]^{1/2}, \quad (3)$$

where $n$ is equal to the number of levels and $p$ is the number of parameters that are varied freely. For fits to the lanthanide ions' energy level structure this value is generally on the order of 10–15 $\mathrm{cm}^{-1}$ but for the actinides $\sigma$ is larger.

In order to compare the magnitudes of the crystal field for different $f^N$ ions in the same host or for a particular $f^N$ ion in different hosts and site symmetries, the quantity $N'_v$, proportional to the scalar crystal field strength parameter $N_v$, defined by Auzel and Malta [6] as

$$N'_v = \frac{N_v}{\sqrt{4\pi}} = \left[ \sum_{k,q} \frac{(B_q^k)^2}{(2k+1)} \right]^{1/2}, \quad (4)$$

is utilized.

Tables 1 and 2 list the values of the free ion and crystal field parameters for the $Cm^{3+}$ ion in a number of single crys-

Table 1
Values of the free ion parameters obtained from fitting the measured energy levels of the Cm(III) ion in five crystals and in 1 M $HClO_4$

| Medium<br>Symmetry | $LaCl_3$[a]<br>$C_{3h}$ | $CsCdBr_3$[b]<br>$C_{3v}$ | $LuPO_4$[c]<br>$D_{2d}$ | $LuPO_4$[d]<br>$D_{2d}$ | $Cs_2NaYCl_6$[e]<br>$O_h$ | $ThO_2$[f]<br>$O_h$ | 1 M $HClO_4$[g] | $Gd^{3+}/LuPO_4$[h]<br>$D_{2d}$ |
|---|---|---|---|---|---|---|---|---|
| $F^2$ | 55338 (61) | 53309 (59) | 54066 (102) | 53674 (359) | 52969 (110) | 50524 (102) | 56608 (167) | 84075 (85) |
| $F^4$ | 44188 (63) | 45993 (91) | 43487 (128) | 41649 (387) | 43888 (181) | 47934 (130) | 44154 | 61411 (106) |
| $F^6$ | 32029 (85) | 31047 (77) | 33078 (126) | 34741 (165) | 30459 (167) | 29271 (84) | 31700 | 44426 (63) |
| $\zeta_f$ | 2881 (6) | 2800 (12) | 2869 (13) | 2924 (6.8) | 2851 (28) | 2691 (14) | 2876.1 (9) | 1494 (10) |
| $\alpha$ | 29.0 (2.0) | 30.2 (4.2) | 27.1 (5.3) | [i] | 24.5 (9.3) | 28.3 | 27.895 (1.2) | 18.9[a] |
| $\beta$ | −313 (25) | −947 (56) | −1270 (54) | [i] | −644 (110) | −650 | 925.21 (137) | −600[a] |
| $\gamma$ | 529 (24) | 864 (58) | 1328 (65) | [i] | 1277 (98) | 825 | 1119.6 (156) | 1575[a] |
| $T^2$ | 167 (34) | 200 | 259 (52) | [i] | 200 | 200 | 100.0 | 300 |
| $T^3$ | 79 (23) | 50 | 50 | [i] | 50 | 50 | 170.0 | 42 |
| $T^4$ | 32 (22) | 40 | 40 | [i] | 40 | 40 | 370.0 | 62 |
| $T^6$ | −346 (28) | −360 | −360 | [i] | −360 | −360 | −300.0 | −295 |
| $T^7$ | 506 (30) | 390 | 390 | [i] | 390 | 390 | 200.0 | 350 |
| $T^8$ | 459 (29) | 340 | 340 | [i] | 340 | 340 | 40.0 | 310 |
| $M^0$ | 1.09 | 1.09 | 1.09 | [i] | 1.09 | 1.09 | 1.09 | 3.22 |
| $M^2$ | 0.608 | 0.61 | 0.61 | [i] | 0.61 | 0.61 | 0.61 | 1.80 |
| $M^4$ | 0.23 | 0.41 | 0.41 | [i] | 0.41 | 0.41 | 0.42 | 1.22 |
| $P^2$ | 1054 | 910 | 912 | [i] | 910 | 912 | 634.9 (96) | 676 |
| $P^4$ | 527.0 | 682.5 | 507 | [i] | 687 | 684 | 497.8 | 507 |
| $P^6$ | 105.4 | 405 | 338 | [i] | 455 | 456 | 354.9 | 338 |

Data for Gd(III)/$LuPO_4$ are given for comparison purposes. Parameters are given in $cm^{-1}$. Parameter values without error values were fixed in the fitting procedures. See references for the full details.

[a] [13].
[b] [15].
[c] [16].
[d] [18].
[e] [92].
[f] [17].
[g] [9] 21 levels were fitted with $\sigma = 48\,cm^{-1}$.
[h] [93].
[i] Not reported.

Table 2
Values of the crystal field parameters obtained from fitting the measured energy levels of the $Cm^{3+}$ ion in five crystals

| Medium<br>Symmetry | $LaCl_3$[a]<br>$C_{3h}$ | $CsCdBr_3$[b]<br>$C_{3v}$ | $LuPO_4$[c]<br>$D_{2d}$ | $LuPO_4$[d]<br>$D_{2d}$ | $Cs_2NaYCl_6$[e]<br>$O_h$ | $ThO_2$[f]<br>$O_h$ | $Gd^{3+}/LuPO_4$[g]<br>$D_{2d}$ |
|---|---|---|---|---|---|---|---|
| $B_0^2$ | 243 (19) | −680 (44) | 503 (41) | 399 (81) | | | 168 (40) |
| $B_0^4$ | −871 (28) | −2237 (66) | 197 (55) | 363 (107) | 4034 (93) | −6446 (43) | 220 (80) |
| $B_3^4$ | | 1894 (53) | | | | | |
| $B_4^4$ | | | −1994 (45) | 2261 (62) | | | −1034 (54) |
| $B_0^6$ | −1232 (33) | −1017 (66) | −3007 (58) | 2470 (132) | 664 (73) | 1142 (32) | −733 (82) |
| $B_3^6$ | | 360 (66) | | | | | |
| $B_4^6$ | | | 626 (55) | 167 | | | 961 (70) |
| $B_6^6$ | 1085 (26) | 935 (56) | | | | | |
| $\sigma$ | 15.7 | 27.3 | 28.4 | 22.3 | 56.7 | 21.7 | 15.5 |
| $n$ (levels)[h] | 103 | 58 | 80 | 47 | 52 | 20 | 44 |
| $N'_v$ | 628 | 1296 | 1302 | | 1836 | 2953 | 657.4 |
| $N'_{vCm}/N'_{vEu}$ | 1.9 | | 2.5 | | 2 | 2.4 | |
| $\Delta E_{max}$ ($^8S_{7/2}$) | 2.02 | 8.0 | 9.52 | | 23[i] | 36 | 0.76 |
| $d_{M-L}$ | 2.95 | | | | 2.54 | 2.42 | |

Data for $Gd^{3+}/LuPO_4$ are given for comparison purposes. Parameters are in $cm^{-1}$ except for the 12th row where $n$ is the number of fitted levels, and the last row where the distances $d$ are in Å. Parameter values without error values were fixed in the fitting procedures.

[a] [13].
[b] [15].
[c] [16].
[d] [92].
[e] [18].
[f] [17].
[g] [93].
[h] Number of levels assigned and fit.
[i] Calculated value.

tals. For comparison purposes the values for the Gd(III) ion are also listed for one crystal. Note that the free ion values for the Cm(III) ion do not change greatly from one host crystal to another nor are they significantly different from the aqueous solution values. However, it should be remembered that the values of the $F^k$ parameters (and the spin–orbit coupling constant) come from the empirical fitting of the calculated energy levels to the observed energy levels. Thus the values obtained for the $F^k$ parameters depend on the number of levels used for the fit, the accuracy of the assignments, the total number of parameters utilized in the fit and the number of parameters permitted to vary independently. In Table 1, the data listed for the values of $F^k$ parameters arise from different studies with quite different numbers of assigned levels. In addition, the measured (and assigned) levels usually are from energies below 40,000 $cm^{-1}$, which cover approximately one quarter of the complete $5f^7$ spectrum for Cm(III). The uncertainties given for the values of the parameters in Table 1 are the statistical uncertainties that arise from the least squares fitting routines. The real uncertainties in the $F^k$ parameters, and also the other parameters used in the fitting routines, are certainly greater than the statistical uncertainties. Given these problems, it is not surprising that there are variations for the values of the $F^k$ parameters for Cm(III) in various matrices and in solution. Note that $F^2$ is the largest of the three $F^k$ parameters, so it should be the best determined.

There are large differences in the free ion parameters between the Cm(III) ion and the Gd(III) ion, most noticeably the $F^k$ parameters are significantly larger for the Gd(III) ion and the spin–orbit coupling $\zeta_{4f}$ is much smaller. This is the expected behavior as the 4f shell is pulled considerably in towards the nucleus for the $4f^N$ series than is the case for the $5f^N$ series resulting in stronger electron repulsion between pairs of equivalent $4f^N$ electrons. As spin–orbit coupling for ions is proportional to the effective nuclear charge Z* to the fourth power, it is much larger for the 5f series ions [7]. Fig. 1 shows how these differences between the two f series affect the free ion energy levels of the Gd(III) and Cm(III) ions. In particular note the enhanced admixture of L–S states of the same $J$ value for the Cm(III) free ion. This admixture is the major reason the crystal field splitting of the ground term is enhanced relative to those found for the Gd(III) ion.

### 2.2. Transition intensities

The intensities of the f–f transitions have been the subject recently of an excellent review. In this section we give the basic equations needed to analyze the intensities of such transitions using the Judd–Ofelt theory following the review and nomenclature of Görller-Walrand and Binnemans [8]. The application of these equations to the Cm(III) ion in solution is then described as given by Carnall and Rajnak [9].

The experimental intensities of an actinide or lanthanide solution spectrum may be determined by the integration of each of the band envelopes in the spectrum. Then it is possible to determine the experimental oscillator strengths $P$ (a dimensionless quantity) in a randomly oriented solution by the following expression:

$$P = 4.32 \times 10^{-9} \int \varepsilon_i(\sigma)\, d\sigma \tag{5}$$

where $\varepsilon_i(\sigma)$ is the molar absorptivity at an energy $\sigma$ in $cm^{-1}$ for each band. The dipole strength $D$ (in units of $esu^2\,cm^2$) for a randomly oriented solution is proportional to the oscillator strength $P$ by the equation

$$D = \frac{(2.127 \times 10^{-30} \times P)}{\bar{\nu}_0} \tag{6}$$

or

$$P = 4.702 \times 10^{29} \times \bar{\nu}_0 \times D \tag{7}$$

where $\bar{\nu}_0$ is the energy of the absorption band baricenter in units of wavenumbers ($cm^{-1}$).

The dipole strength $D$ for a randomly oriented sample is defined as

$$D = \frac{1}{3} \times \left[ (\Psi_i|o_x|\Psi_j)^2 + (\Psi_i|o_y|\Psi_j)^2 + (\Psi_i|o_z|\Psi_j)^2 \right] \tag{8}$$

where $o_i$ is either the magnetic dipole or electric dipole operator with its direction $i$ oriented with the $x$, $y$ or $z$ directions of the $f^N$ complex. $\Psi_i$ and $\Psi_j$ represent the initial and final state wavefunctions of the transition.

The experimental dipole strength (or the experimental oscillator strength) can be compared with the total calculated dipole strength (where ED and MD are electric dipole and magnetic dipole respectively) for a randomly oriented system as follows:

$$D_{\text{exp}} = \frac{1}{2J+1}(\chi_{\text{MD}} D_{\text{MD}} + \chi_{\text{ED}} D_{\text{ED}}) \tag{9}$$

where $\chi_{\text{MD}}$ and $\chi_{\text{ED}}$ are related to the dielectric constant of the isotropic medium in which the compound or complex is situated. These correction factors are different for absorption and emission processes, and are given by the following:

$$\text{Absorption}: \quad \chi_{\text{ED}} = \frac{(n^2+2)^2}{9n}, \qquad \chi_{\text{MD}} = n \tag{10}$$

$$\text{Emission}: \quad \chi_{\text{ED}} = \frac{(n^2+2)^2}{9}, \qquad \chi_{\text{MD}} = n^3 \tag{11}$$

and $n$ is the dielectric constant of the medium.

Application of the Judd–Ofelt theory [10,11] as formulated by Axe [12] allows the matrix elements for the electric dipole operator to be evaluated from

$$D_{\text{exp}}(\text{ED}) = \frac{\chi_{\text{ED}}}{2J+1} \times \left[ e^2 \sum_{k=2,4,6} \Omega_k \langle \Psi J | U^{(k)} | \Psi' J' \rangle \right]^2 \tag{12}$$

Here, $\Psi J$ and $\Psi' J$ refer to the initial and final states within an $f^N$ configuration. The $\Omega_k$ parameters are evaluated from the experimental band intensities and contain contributions from excited configurations of opposite parity, such as the $f^{N-1}d$ configuration, and also from ligands in the immediate environment.

The matrix elements in Eq. (12) and in all the equations in this paper are sums over all the LS states that comprise the ground state and excited state wavefunctions that are obtained

by the diagonalization of Eq. (1) with the empirical values of the parameters in that equation obtained by fitting the observed energies. Thus intermediate coupled wavefunctions should be used in the expressions for $\langle \Psi J|$ and $|\Psi' J'\rangle$. Thus each $\langle \Psi J|$ is a summation of the type:

$$\langle \Psi J| = \varphi(\hat{S}\hat{L}J) = \sum_{\alpha SL} x(\alpha SLJ)\psi(\alpha SLJ) \tag{13}$$

where $x(\alpha SLJ)$ is the component of the eigenvector of the unperturbed state $\psi(\alpha SLJ)$ and $\hat{S}\hat{L}$ are labels of the intermediate-coupled wavefunction [5].

Magnetic dipole transitions may be calculated from

$$D(\mathrm{MD}) = \frac{e^2\left(\frac{h}{2\pi}\right)^2}{4m^2c^2}\langle \Psi J|L + 2S|\Psi' J'\rangle^2. \tag{14}$$

In this case the transitions are allowed within an $f^N$ configuration so these matrix elements are easily obtained. When fitting the Judd–Ofelt ($\Omega_k$) parameters to the experimental intensities of $f \rightarrow f$ transitions, the calculated intensities of the magnetic dipole transitions must first be subtracted from the experimental intensities in order to obtain the correct values of the $\Omega_k$ parameters [9].

### 2.3. Radiative and non-radiative decay processes

The spontaneous emission coefficient or the Einstein coefficient for spontaneous emission, $A(\Psi J, \Psi' J')$ in $s^{-1}$, is defined as follows:

$$A(\Psi J, \Psi' J') = \frac{64\pi^4\bar{\nu}^3}{3h(2J+1)}\left[n^3 D_{\mathrm{MD}} + \frac{n(n^2+2)^2}{9}D_{\mathrm{ED}}\right] \tag{15}$$

This equation implicitly assumes that all crystal field levels of the initial state $\langle \Psi J\rangle$ are equally populated. In principle an excited state can relax to different lower-lying levels, $\langle \Psi' J'\rangle$ so that the branching ratio $\beta_{\mathrm{R}}$ is defined as

$$\beta_{\mathrm{R}}(\psi J, \psi' J') = \frac{A(\Psi J, \Psi' J')}{\sum_{\psi' J'} A(\Psi J, \Psi' J')} \tag{16}$$

The emission coefficients can be calculated from the Judd–Ofelt ($\Omega_k$) parameters for each of the luminescent transitions from a particular excited level and compared with the experimental value obtained from lifetime measurements. The radiative lifetime $\tau_{\mathrm{R}}$ for the level $\langle \Psi J\rangle$ is given by

$$\tau_{\mathrm{R}}(\Psi J) = \frac{1}{\sum_{\Psi' J'} A(\Psi J, \Psi' J')} \tag{17}$$

The difference between the experimental value and the value calculated from the $\Omega_k$ parameters can be attributed to relaxation processes that shorten the radiative lifetime, that is non-radiative processes such as energy transfer to acceptor molecules within the direct neighborhood of the excited ion. For effective energy transfer the acceptor level should be no lower than a few times the maximum phonon frequency of the system. Such quenchers could be ligand-to-metal charge transfer bands or ligand $\pi^*$ levels of complexed aromatic ligands, transition metal ions with low lying d- or f-states (such as Fe(III), Nd(III)) within the Förster-radius of about 1 nm. In the absence of such acceptor molecules multiphonon-decay via high-frequency vibrations of molecules in the first or second coordination shell may be effective. For lanthanide ions, the non-radiative decay rate $W_{\mathrm{T}}(\Psi J)$ are mainly temperature dependent processes following the expression:

$$W(T) = W(0)\left[\frac{\exp(\hbar\omega_{\mathrm{m}}/kT)}{\exp(\hbar\omega_{\mathrm{m}}/kT) - 1}\right]^{\Delta E/\hbar\omega_{\mathrm{m}}} \tag{18}$$

where $\hbar\omega_{\mathrm{m}}$ is the maximum phonon energy of the lattice vibration, $\Delta E$ the energy gap between the emitting level and the next low lying state and $W(0)$ is the spontaneous transitions state at $T = 0$. At low temperature, where $\hbar\omega_{\mathrm{m}} \gg kT$, the non-radiative relaxation rate can be expressed by the exponential energy gap law

$$W(0) = C\,\exp\left(\frac{-\alpha\Delta E}{\hbar\omega}\right) \tag{19}$$

where $C$ and $\alpha$ are empirical parameters characteristic of the media.

Few studies of relaxation processes for actinide ions have been published. Nevertheless, it has been shown that electron–phonon coupling is stronger for Cm(III) in $LaCl_3$ than for lanthanides in this host [13]. Phonon energies in dielectric crystals are primarily dependent on the ligands in the first coordination sphere and vary from 180 $cm^{-1}$ (for bromide) to 1100 $cm^{-1}$ (for phosphate), thus multiphonon processes are less important for heavy ligands. However, molecules with hydrogen bonds such as OH, NH or CH with vibrational stretching frequencies of 3000–3500 $cm^{-1}$ are very efficient quenchers if the molecule is directly coordinated to the Cm(III).

Finally, the quantum efficiency per excited ion $\eta$ is defined as

$$\eta = \frac{\tau_{\mathrm{meas}}(\Psi J)}{\tau_{\mathrm{R}}(\Psi J)} \tag{20}$$

## 3. Spectroscopic properties of Cm(III) in solids

### 3.1. Electronic structure

The electronic structure of Cm(III) has been investigated in optical crystals with non-cubic sites such as $LaCl_3$, $LuPO_4$ and $CsCdBr_3$ [13–16] as well as in centrosymmetric systems such as $ThO_2$ and $Cs_2NaYCl_6$ [17,18] using absorption and laser selective excitation and fluorescence spectroscopy. The most complete analysis of the Cm(III) optical spectrum to date is for Cm(III) in $LaCl_3$ with 103 assigned experimental energy levels and for which very good agreement (20 $cm^{-1}$) was obtained between calculated and experimental levels. The use of excited state absorption spectroscopy (ESA) utilizing the $^6D_{7/2}$ metastable emitting level pumped with two visible lasers, allowed the experimental characterization of levels up to 40,000 $cm^{-1}$ with high resolution [13,15,16]. The observed energy levels were deduced from electric (or magnetic) dipole

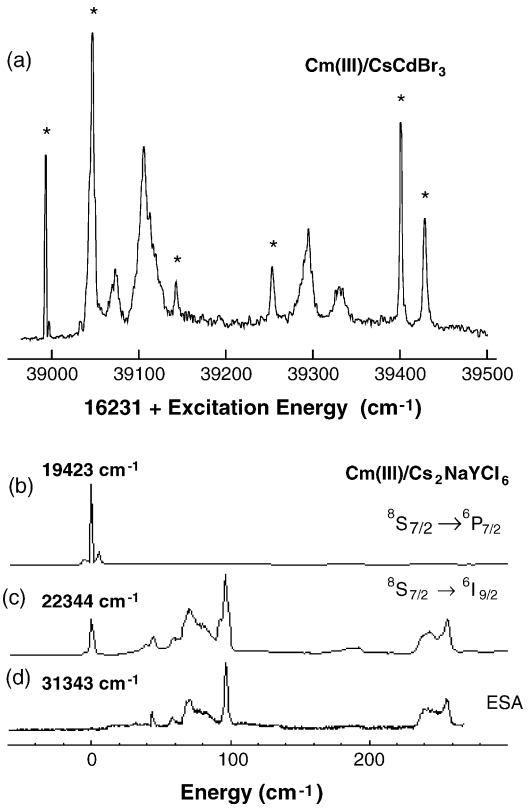


Fig. 2. Excitation spectra showing (a) excited state absorption in Cm(III)/$CsCdBr_3$ at ~10 K with pumping of the $^6D_{7/2}$ state at 16,231 $cm^{-1}$ and a second tunable visible laser used for excitation. The asterisk (*) represents lines also seen with the pumping laser blocked. See Ref. [15] for details, (b–d) show the zero-phonon lines and vibronic structure observed at ~10 K in Cm(III)/$Cs_2NaYCl_6$. One photon excitation spectra were used for (b) and (c) and excited state absorption of the $^6D_{7/2}$ state was utilized for (d). See Ref. [18] for details.

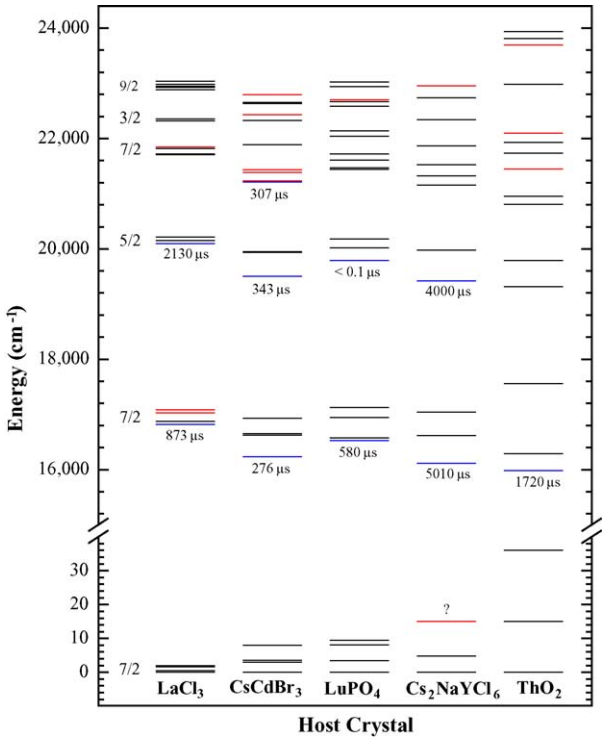


Fig. 3. Low lying crystal field levels of $Cm^{3+}$ in several host lattices. The electronic levels are measured at 4.2 K. The numbers given indicate the fluorescent lifetime of some emitting levels. The *J* multiplets are indicated on the left-hand side.

transitions between the $^8S_{7/2}$ ground state and the electronic excited states using conventional one photon spectroscopy and also two photon spectroscopy techniques such as ground state excitation (GSE) and excited state absorption (ESA). Fig. 2a shows an example of ESA in the Cm(III)/$CsCdBr_3$ system.

For centrosymmetric sites in crystals, Cm(III) optical spectra are primarily dominated by vibrational transitions (zero-phonon electric dipole transitions are forbidden) and allowed zero-phonon magnetic dipole transitions. In these systems the optical spectra have strong vibronic features, so the zero-phonon transitions and vibronic bands must be distinguished. Fig. 2b–d show examples of excitation spectra of the Cm(III) at an $O_h$ centrosymmetric site using either ESA spectroscopy or laser selective excitation, where vibrational transitions can be dominant. Note the vibronic bands are usually broad when composed of superimposed vibronic transitions, while the zero-phonon lines are very narrow. The energies of the zero-phonon electronic transitions in some cases can be derived from the assignments of the vibronic bands.

Selected electronic energy levels for Cm(III) measured in various crystals are compared in Fig. 3. The Cm(III) ion experiences different crystal field strengths and site symmetries in these systems with an increase of the crystal field strength from the left to the right. $LaCl_3$ produces the weakest CF strength with a ground state multiplet splitting of only 2 $cm^{-1}$ while the cubic site of $ThO_2$ induces the largest CF strength with a total $^8S_{7/2}$ splitting of about 40 $cm^{-1}$. Simultaneously the total splitting of the other *J* multiplets is increasing from $LaCl_3$ to $ThO_2$. The crystal field strength decreases as the M–L bond distance increases (see Table 2).

### 3.2. Crystal field strength

As mentioned earlier, the scalar parameter $N'_v$ is a commonly used parameter to evaluate the magnitude of the total crystal field strength of an ion in different hosts. This parameter provides a useful means for determining crystal field effects on different $f^N$ ions in the same matrix or the effect of different matrices with the same ion. It has been shown that the ratio of $N'_v$ between an $5f^N$ ion and its lanthanide analog is approximately constant and of the order of $2.2 \pm 0.2$ for Cm(III) in a series of different host crystals [15,17,18] confirming that crystal field strength of trivalent actinides is twice as strong as for the lanthanide analog.

Auzel and Malta [6] showed that this parameter gives a linear relationship with $\Delta E_{max}$, the maximum Stark (crystal field) splitting of *J*-terms with small *J*-mixing as shown by the expression:

$$\Delta E_{max} \propto \left[ \prod_k \left\langle J \left\| \sum_i C_i^k \right\| J \right\rangle \right]^{1/3} N'_v. \quad (21)$$

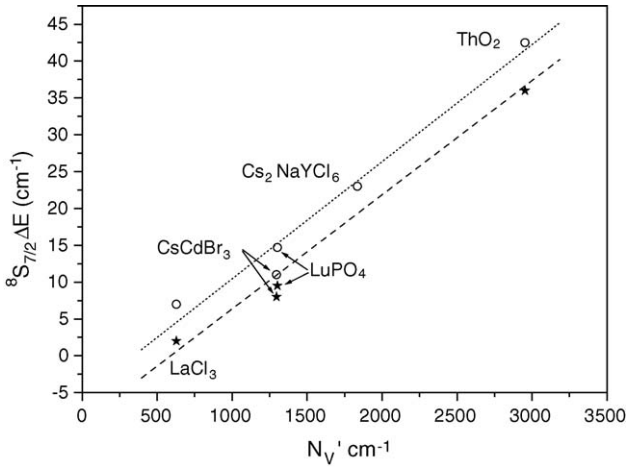


Fig. 4. Maximum stark splitting of the $^8S_{7/2}$ multiplet vs. $N'_v$ for $Cm^{3+}$ in several host matrices. Dotted line corresponds to linear fit from calculated values (◯) and dashed line to linear fit from experimental values (⋆).

For the ground $^8S_{7/2}$ multiplet of Cm(III), *J*-mixing is very small. Fig. 4 shows the variation of the $N'_v$ parameter calculated for Cm(III) in selected crystals with the total ground multiplet splitting $\Delta E_{max}(^8S_{7/2})$ for these systems is linear. Note that in all cases the calculated $\Delta E_{max}(^8S_{7/2})$ splitting is systematically higher than the experimental values with roughly the same slope. For these systems the cubic site symmetry hosts induce the largest crystal field. Edelstein and Easley [19] also found a large ground multiplet splitting in the cubic host $CaF_2$ (estimated at 35.7 $cm^{-1}$). From this linear variation, a measurement of the total $^8S_{7/2}$ ground-multiplet splitting of Cm(III) can provide an estimate of the magnitude of crystal field strength in that system.

### 3.3. Fluorescence lifetime of the Cm(III) ion in solids

Among all the trivalent actinides, the Cm(III) fluoresces most strongly due to its large energy gap between the first $^6D_{7/2}$ excited state level and the low lying ground multiplet $^8S_{7/2}$ ($\Delta E > 16{,}000\ cm^{-1}$). However, in halide crystals (chloride or bromide) doped with very low concentrations of Cm(III) ($10^{-3}$–$10^{-5}$ atom%), the energy cut-off of the phonon spectrum is only few hundred $cm^{-1}$ ($\hbar\omega_m < 300\ cm^{-1}$) and all states with energy gaps $\geq 1200\ cm^{-1}$ fluoresce at low temperatures. These data are given in Table 3. The measured lifetimes of the first $^6D_{7/2}$ excited state varies from 276 μs in $CsCdBr_3$ to 5010 μs in $ThO_2$ at liquid helium temperature. The measured lifetimes of the emitting levels with energy gaps of about 16,000 $cm^{-1}$ are dominated by the radiative relaxation process, and can be considered to be close to the radiative decay rate from the lowest $^6D_{7/2}$ crystal field state.

The shortest measured lifetime of the $^6D_{7/2}$ crystal field state occurs in $CsCdBr_3$. The major spectral features in this system are from two Cm(III) ions substituting for three Cd(II) ions with a Cd(II) vacancy located between the two Cm(III) ions. This particularly short lifetime can be explained by energy transfer between this pair of Cm(III) ions. However, the significant temperature dependence found for the $^6D_{7/2}$ level in all the crystal lattices and especially for the elpasolite system is an unexpected result and cannot be from purely radiative decay. This quenching is probably due to impurity ion cross relaxation.

Radiative processes are the preferred relaxation pathway only for the $^6D_{7/2}$ and $^6P_{7/2}$ states in the halide crystals. The lifetimes of the other emitting levels of Cm(III) in these solids, the $^6I_{7/2}$, $^6I_{11/2}$, $^6I_{17/2}$, $^6D'_{7/2}$ and $^6G_{5/2}$ levels, have smaller energy gaps to the next lowest level but always larger than 1200 $cm^{-1}$. Lifetimes are shorter and non-radiative multiphonon relaxation processes compete with radiative decay. For Cm(III) in $LuPO_4$ and $ThO_2$ crystals for which the vibrational spread is larger (see Table 3), only one or two levels fluoresce. A comparison of the use of the energy gap law (Eq. (19)) for Cm(III) and the lanthanides in $LaCl_3$ has been reported [13]. The ion-phonon coupling for Cm(III) was found to be stronger than for lanthanides in $LaCl_3$ as expected.

### 3.4. Nephelauxetic effect in Cm(III) compounds from fluorescence shifts

The nephelauxetic effect for transition metals of both the f and d series is characterized by a shift of a particular optical transition to lower energy by the ion in a condensed phase (solution or solid) when compared with the same transition for the gas phase free ion. The magnitude of the shift is correlated with the extent of covalent bonding with the ligands defining the first coordination sphere of the ion in the condensed phase. The nephelauxetic effect, defined as the ratio of the electrostatic (Slater) parameters of the ion in a compound or complex to that of the free ion, has been utilized as a measure of covalent effects. For the trivalent actinide ions there are three Slater parameters and it is common to use the decrease in the $F^2$ Slater parameter as the measure of this effect. However, for the trivalent actinides, for the most part, the free ion gas parameters are unknown. Instead the free ion parameters obtained for the aqueous ion are utilized as the standard.

Barbanel' [20] has utilized the absorption transition of the Am(III) ion from the ground $J = 0$ multiplet to the $^5L_0$ multiplet to arrange a number of Am(III) compounds into a nephelauxetic series of systems. The Am(III) compounds differ in the types of ligands, and in cases where the ligands are the same, the coordination geometry and the bond lengths are different. In the latter case the phase, coordination number, symmetry and temperature are factors that may affect the ordering. The usual ordering of the ligands (where the smallest effect signifies the least change of the electrostatic parameters) is $F^- < H_2O < Cl^- < Br^- < O_2^- < C_2H_5^-$. Barbanel' found two cases where the data did not follow the above order. In one case, $AmF_6^{3-}$ in a CsF/NaF melt at 833 K, showed a larger nephelauxetic effect than Am(III) aqueous ion at room temperature. In the second case $Br^- < Cl^-$ for a series of octahedral $AmX_6^{3-}$ compounds. In both cases Barbanel' [20] pointed out there was a large decrease in coordination number with a corresponding decrease in bond lengths before this inversion of anions occurs.

For Cm(III) fluorescence shifts, what is observed is the transition from the lowest energy crystal field level of the first excited $^6D_{7/2}$ multiplet to the ground multiplet of the $^8S_{7/2}$ state. The

Table 3
Fluorescent lifetimes for Cm (III) in various crystalline host matrices

| Multiplet | $^6D_{7/2}$ | $^6P_{5/2}$ | $^6I_{7/2}$ | $^6I_{11/2}$,$^6I_{17/2}$ | $^6D'_{7/2}$ | $^6G_{5/2}$ |
|---|---|---|---|---|---|---|
| $Cm^{3+}/CsCdBr_3$[a] | | | | | | |
| Energy ($cm^{-1}$) | 16231 | 19502 | 21214 | 24264 | 27540 | 29011 |
| 4.2 K lifetime (μs) | 276 (30) | 343 (30) | 307 (30) | 143 (15) | 75 (10) | 57 (6) |
| Energy gap[b] ($cm^{-1}$) | 16223 | 2575 | 1267 | ∼1500 | ∼1390 | ∼1350 |
| $\hbar\omega_m$ ($cm^{-1}$) | 180 | | | | | |
| $Cm^{3+}/LaCl_3$[c] | | | | | | |
| Energy ($cm^{-1}$) | 16815 | 20095 | | 24990 | 28068 | 29645 |
| 4.2 K lifetime (μs) | 815 (10) | 2120 (20) | | 292 (5) | 115 (5) | 32 (3) |
| 295 K lifetime (μs) | 530 (10) | 960 (10) | | 151 (5) | 53 (5) | 11 (2) |
| Energy gap[b] ($cm^{-1}$) | 16183 | 3014 | | 1955 | 1503 | 1481 |
| $\hbar\omega_m$ ($cm^{-1}$) | 250 | | | | | |
| $Cm^{3+}/Cs_2NaYCl_6$[d] | | | | | | |
| Energy ($cm^{-1}$) | 16117 | 19423 | | 24218 | 27670 | |
| 4.2 K lifetime (μs) | 5010 (10) | 4050 (10) | | 94 (5) | 9.9 (1.0) | |
| 295 K lifetime (μs) | 240 (5) | 236 (5) | | – | – | |
| Energy gap[b] ($cm^{-1}$) | ∼16000 | 2377 | | ∼1270 | ∼1380 | |
| $\hbar\omega_m$ ($cm^{-1}$) | 300 | | | | | |
| $Cm^{3+}/ThO_2$[e] | | | | | | |
| Energy ($cm^{-1}$) | 15984 | 19315 | 20828 | (23690) | (27149) | |
| 4.2 K lifetime (μs) | 1860 (10)[f] | | | | | |
| 295 K lifetime (μs) | 1380 (10)[g] | | | | | |
| Energy gap[b] ($cm^{-1}$) | 15948 | 1761 | 1021 | ∼708 | ∼954 | |
| $\hbar\omega_m$ ($cm^{-1}$) | 560 | | | | | |
| $Cm^{3+}/LuPO_4$[g] | | | | | | |
| Energy ($cm^{-1}$) | 16528 | 19777 | | | | |
| 4.2 K lifetime (μs) | 580 | ∼0.100 | | | | |
| Energy gap[b] ($cm^{-1}$) | 16519 | 2656 | | | | |
| $\hbar\omega_m$ | 1100 | | | | | |

[a] [13].
[b] To the next lowest level.
[c] [15].
[d] [18].
[e] [17].
[f] [94].
[g] [16].

splitting of the ground multiplet is small, for the most part on the order of 10–20 $cm^{-1}$ and can be neglected. However, the crystal field splitting of the excited $^6D_{7/2}$ multiplet is of the order of 300–600 $cm^{-1}$. Since the nephelauxetic effect is essentially a free ion phenomenon, it is necessary to correct luminescence spectra for the crystal field splitting. As shown earlier and also in Table 4 this can be done if the energies of the four crystal field levels of $^6D_{7/2}$ state are known or can be estimated from fits or data at other temperatures. The centers of gravity for this multiplet are shown in column 6 of Table 4 for a number of systems.

The systems can be divided into four groups from the values of the observed fluorescence lines given in column 4 of Table 4. The first group (smallest shift) contains the aqueous ions, both in solution and in solids, the 9 coordinate curium chloride compounds and the high coordination number compound $CmF_3$. The second group comprises the Cm(III) phosphate compounds and $CmBr_3$. The third group includes Cm(III) diluted in $CsCdBr_3$, $CmI_3$ and Cm(III) in the chloroelpasolites. The Cm(III) in $ThO_2$ data indicate a slightly larger shift than found in the third group followed by $Cm(C_5H_5)_3$ with the largest shift of all the Cm(III) samples. This qualitative ordering is approximately the same as found by Barbanel' [20] in his study of Am(III) compounds. It should be noted that from the data in Table 4, column 4, the $CmF_3$ compound is placed with Cm(III)/$LaCl_3$, $CmCl_3$ and a Cm(III) crystalline compound that has 8 $H_2O$ in the first coordination sphere, contrary to the expected nephelexautic effect.

If corrections are made for the crystal field splitting of the $^6D_{7/2}$ multiplet (Table 4, column 6) the first group stays approximately the same (assuming the $CmF_3$ center of gravity would be at least ∼200 $cm^{-1}$ higher). Interestingly, the value of the center of gravity of crystalline $[Cm(H_2O)_9](III)$ compound agrees quite well with the assignment of this same transition in the absorption spectrum. In the second group by this criteria are the phosphate crystals and $CmBr_3$. The Cm(III)/$CsCdBr_3$ dimer with a trigonally distorted octahedral array of $Br^-$ ions around each Cm(III) ion follows. With this criterion the Cm(III) ion in the chloroelpasolite and Cm(III) in $ThO_2$ are at approximately the same energy although the latter system shows a slightly larger red shift. Using the value of the baricenter for the $^6D_{7/2}$ multiplet for $Cm(C_5H_5)_3$ of 15,920 $cm^{-1}$ [21] shows this compound still has the largest shift of all the systems in Table 4.

Table 4
Cm (III) data in various systems illustrating the nephelauxetic effect (see text for detailed explanation)

| Sample | Form, temperature[a] | $Cm^{3+}$ coordination | Fluorescence ($cm^{-1}$) | Total splitting $^6D_{7/2}$ ($cm^{-1}$) | Center of gravity $^6D_{7/2}$ ($cm^{-1}$) | $F^2$ ($cm^{-1}$) | Reference |
|---|---|---|---|---|---|---|---|
| $Cm^{3+}/HClO_4$ | Sol. RT | ~9 $H_2O$ | 17089[b] | | | 56608 | [9] |
| $Cm^{3+}$(aq) | Sol. RT | ~9 $H_2O$ | 16863 | | | | [2] |
| $[Cm(H_2O)_9]^{3+}$ | Crystal RT. | $C_{3h}$ 9 $H_2O$ | 16850 | 540 | 17088 | | [24] |
| $Cm^{3+}$(aq) | Sol. RT | ~9 $H_2O$ | 16840 | | | | [24] |
| $Cm/LaCl_3$ | Crystal 10 K | $C_{3h}$ 9 $Cl^-$ | 16815 | 266 | 16951 | 55338 | [13] |
| $CmCl_3$ | Polycrys. 77 K | $C_{3h}$ 9 $Cl^-$ | 16759 | ~389 RT | ~16977 | | [95] |
| $CmF_3$ | Polycrys. 77 K | 11 $F^-$ tricapped trigonal coord. | 16751 | | | | [95] |
| $[Cm\ (H_2O)_8]^{3+}$ | Crystal RT | 8 $H_2O$ | 16742 | 678 | 16984 | | [24] |
| $Cm/YPO_4$ | Crystal 10 K | 8 O $D_{2d}$ | 16581 | 601 | 16834 | 52544 | [92] |
| $CmBr_3$ | Polycrys. 77 K | 8 $Br^-$ distorted cubic | 16579 | 278 (483 RT) | 16757 | | [95] |
| $Cm/LuPO_4$ | Crystal 10 K | 8 O $D_{2d}$ | 16528 | 596 | 16786 | 54066, 53674 | [16,92] |
| $Cm/CsCdBr_3$ | Crystal 10 K | 6 $Br^-$ trigonally distorted $O_h$ | 16231 | 696 | 16608 | 53309 | [15] |
| $CmI_3$ | Polycrys. 77 K | 6$I^-$ distorted $O_h$ | 16213 | 406 | 16411 | | [95] |
| $Cm/Cs_2NaLuCl_6$ | Crystal 77 K | 6$Cl^-$ $O_h$ | 16122 | | | | [96] |
| $Cm/Cs_2NaYCl_6$ | Crystal 10 K | 6$Cl^-$ $O_h$ | 16117 | 1042 | 16579 | 52969 | [18] |
| $Cm^{3+}/ThO_2$ | Polycrys. 10 K | 8 $O^{2-}$ cubic | 15984 | 1543 | 16529 | 50524 | [17] |
| Cm $(C_5H_5)_3$ | Polycrys. RT | ~$C_{3v}$ with 3 $[C_5H_5]^-$ centroids | 15490 | | 15920 | | [21] |

[a] RT, room temperature; sol., aqueous solution; polycrys., polycrystalline solid.
[b] This transition energy is from an absorption measurement.

Finally, for a number of the systems listed in Table 4 fits of the observed energy levels have been given. Values of the free ion parameter $F^2$ are given in Table 4, column 7. Qualitatively, the lower the value of $F^2$, the greater is the nephelauxetic effect. By this criterion, for the systems where data are available, the order follows that of the fluorescence data, except for Cm(III)/$YPO_4$, which appears to have a rather low value of $F^2$ placing this system below Cm(III)/$Cs_2NaYCl_6$. It is also odd that this value of $F^2$ is so different that that found for Cm(III)/$LuPO_4$, a very similar system.

In summary, the shifts to lower energy of the fluorescence for Cm(III) systems qualitatively follow the trends expected for the nephelauxetic effect. However, as shown by Barbanel' for Am(III) systems and also found for Cm(III) systems, when low coordination and strong crystal fields are encountered in actinide systems, there are some reversals found in the usual order of anions. Nevertheless, it is clear that the major factor causing the red shifts for Cm(III) systems is the diminution of electrostatic repulsion effects at the Cm(III) ion due to ligand interactions.

## 4. Spectroscopy of the Cm(III) aquo ion

### *4.1. Absorption and emission spectra of the Cm(III) aquo ion*

Carnall and Rajnak [9] published the optical absorption spectrum of Cm(III) (using either $^{244}Cm$ and $^{248}Cm$ isotopes) in 1 M $HClO_4$ (Fig. 5). Solution spectra were carefully measured to ~40,000 $cm^{-1}$ in 1 cm cells. Band envelopes were integrated and the experimental oscillator strengths were determined using Eq. (5). The free ion energy levels were calculated using the free ion Hamiltonian (Eq. (1)) and the initial parameters extrapolated from earlier analyses of neighboring An(III) ions. After assignment of the bands, a number of free ion parameters were allowed to vary simultaneously with others being determined by fixed ratios or extrapolated from neighboring ions. From the wavefunctions determined by this fit the $U^{(k)}$ matrix elements necessary to fit the $\Omega_k$ parameters given in Eq. (8) and the magnetic dipole transition intensities were obtained. The experimental data and intensity fit obtained by Carnall and Rajnak [9] are shown in Fig. 5. The Judd–Ofelt $\Omega_k$ parameters are given in Table 5.

Using the above equations and the Carnall and Rajnak values of the $\Omega_k$ parameters given in Table 5, the radiative lifetime for the $^6D_{7/2}$ multiplet at 17,095 $cm^{-1}$ can be calculated. The value obtained is $\tau_R = 1.4$ ms. It should be noted that there is a rather large error associated with this number, on the order of 65%, because of the large error associated with the $\Omega_2$ value of $15.2(9.9) \times 10^{-20}$ $cm^2$.

The first solution emission spectrum of Cm(III) was reported in 1964 by Gutmacher et al. [22] in a 10 M LiCl aqueous solution excited by the alpha decay of $^{244}Cm$ (18.1 year half-life),

Table 5
Values of the Judd–Ofelt intensity parameters and the $U^{(k)}$ matrix elements from the ground multiplet to the first excited multiplet at 17,095 $cm^{-1}$ (from Ref. [9])

| Parameter or matrix element | Value |
|---|---|
| $\Omega_2$ ($10^{-20}$ $cm^2$) | 15.2 (9.9) |
| $\Omega_4$ ($10^{-20}$ $cm^2$) | 16.8 (2.6) |
| $\Omega_6$ ($10^{-20}$ $cm^2$) | 38.1 (1.0) |
| $U^{(2)}$[a] | 0.0264 |
| $U^{(4)}$[a] | 0.0080 |
| $U^{(6)}$[a] | 0.0054 |

[a] $U^{(k)} = \langle \Psi J || U^{(k)} || \Psi' J' \rangle^2$.

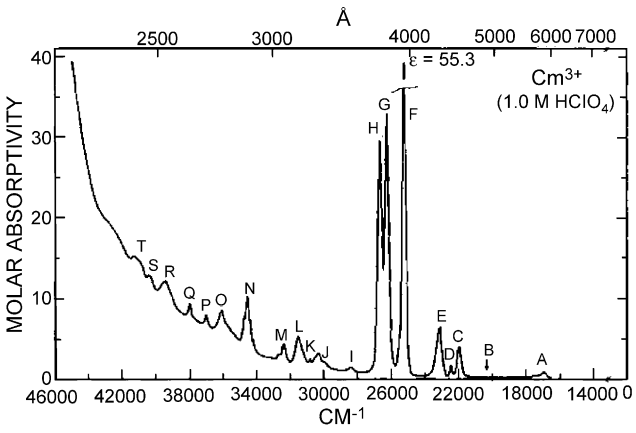


| Band | 2J | E(cm$^{-1}$)[a] Center | Px10$^6$ Obs'd | Px10$^6$[b] Calc'd |
|---|---|---|---|---|
| A | 7 | 17095 | 1.6 | {2.0 E.D. 0.2 M.D. |
| B | 5 | 20350 | 0.4 | {0.6 E.D. 0.2 M.D. |
| C | 7 | 21955 | 5.7 | 4.7 |
| D | 3 | 22435 | 0.7 | 0.01 |
| E | 9 | 23120 | 11 | 10 |
| F | {17, 11} | 25250 | 49 | 52 |
| G | {9, 13} | 26225 | 40 | 37 |
| H | 15 | 26630 | 35 | 34 |
| I | 7 | 28370 | 1.0 | 2.0 |
| J | 5 | 30030 | 1.1 | 1.1 |
| K | {7, 5, 3} | 30550 | 3.6 | 4.3 |
| L | 11 | 31500 | 8.2 | 9.5 |
| M | {9, 3} | 32500 | 3.2 | 5.3 |
| N | 13 | 34540 | 12 | 8.4 |
| O | {17, 7, 11, 9, 13, 1} | 35800 | 4.0 | 6.0 |
| P | 7 | 37010 | 1.2 | 0.3 |
| Q | 5 | 37995 | 2.0 | 0.6 |
| R | {15, 3, 13, 5, 9} | 39400 | ~10[c] | 5.1 |
| S | {11, 7} | 40300 | ~1.6[c] | .44 |
| T | {5, 9, 15, 11} | 41100 | ~10[c] | 1.8 |

R.M.S. Deviation = 1.9 x 10$^{-6}$

[a] When two or more free ion levels were included in an unresolved band an average energy is indicated. See [9] for the calculated and assigned levels.

[b] Parameters used to obtain these values are given in Table 1.

[c] These values were not included in the set used to determine the intensity parameters.

Fig. 5. Absorption spectrum of $^{248}Cm^{3+}$ in 1.0 M $HClO_4$. Assignments, and experimental and calculated oscillator strengths are given after the figure. The figure and data are taken directly from Ref. [9]. Reprinted with permission, Copyright 1975, American Institute of Physics.

i.e. autoradioluminescence. Beitz and Hessler [2] obtained the first optically excited luminescence spectrum of the Cm(III) aquo ion in their pioneering paper on the use of optical spectroscopy for the speciation of actinides in natural aquatic systems in the context of nuclear waste disposal in geological formations. They discussed the need for highly sensitive methods applicable to actinide speciation at sub-micro-molar concentrations, and estimated a limit of detection (LOD) for Cm(III)(aq) in 0.1 M $HClO_4$ of about $3 \times 10^{-13}$ mol/L based on their emission measurements. They also discussed the potential of the methods not only to derive information about the oxidation state but also about the molecular structure.

The emission spectrum of Cm(III)(aq) at room temperature is shown in Fig. 6 (left side) and compared with the spectra of hydrolysed Cm(III). In aqueous solution only emission from the first excited state $^6D_{7/2}$ is observed. The spectrum consists of a single peak with a maximum at 593.8 nm (16,840 $cm^{-1}$) and a FWHM of 7.7 nm. Because the crystal field splitting of the $^6D_{7/2}$ excited state is on the order of several 100 $cm^{-1}$, the spectrum is asymmetrically broadened at the higher energy (blue)-side by unresolved hot bands. The ground state splitting is on the order of several $cm^{-1}$ and individual crystal field transitions are not resolved. Features from the lowest crystal field state of the excited multiplet are dominant in the emission spectra at room temperature, so the spectral sensitivity to the nephelauxetic and ligand field effects are different than those obtained from solution absorption spectra.

Solution fluorescence of Cm(III) is best excited at the intense absorption maxima of the F, G or H bands in the near UV (see Fig. 5) using pulsed tunable lasers sources. Excitation spectra in this wavelength range correspond to the absorption spectra, but with much better sensitivity compared to the usual absorption spectroscopy. In the case of energy transfer from an absorbing ligand to Cm(III) a superposition of direct Cm(III) and ligand absorption can be observed (see Section 6.3). Ligand to metal energy transfer not only increases the emission intensity (sensitized fluorescence) but also provides valuable information on the Cm(III) coordination.

### 4.2. Cm(III) lifetime and determination of hydration number

Beitz and Hessler [2] reported the first observation of the lifetime of the Cm(III) ion fluorescence in solution in 1980. They measured a fluorescence lifetime of 65 ± 2 μs for the 593 nm emission in 1 M HCl or 0.1 M $HClO_4$ at room temperature. The measured lifetime (single exponential) in ~0.5 M DCl or 0.1 M $DClO_4$ (99% D atom) was 940 ± 20 μs at room temperature (295 ± 1 K). Kimura et al. [23] have also published the lifetimes of Cm(III) in 0.01 M $HClO_4$ and $D_2O$ (99.95%) at room temperature with the values 65 ± 2 and 1200 ± 30 μs. A recent paper describing Cm(III) hydration in aqueous solution from 20 to 200 °C has been published. Lindqvist-Reis et al. [24] report values of 64 ± 3 and 1370 ± 40 μs for 20 °C in $H_2O$ and $D_2O$, respectively.

Liu and Beitz [25] have pointed out that when the difference in the degree of deuteration between the deuterated water used by Beitz and Hessler [2] and that used by Kimura et al. [23] is taken into account, the agreement between the Cm(III) lifetimes measured in the two different deuterated aqueous solutions is satisfactory at the 95% confidence level.

Horrocks and Sudnick [26] studied the relaxation rates of the Eu(III) (and of the Tb(III)) ion in aqueous solution and determined the correlation between the number of water molecules in the first coordination sphere and the Eu(III) fluorescence lifetime. They calibrated their correlation by using crystalline compounds of known X-ray structure with a variable number of water molecules in the first coordination sphere about the Eu(III) ion. In their model it was assumed the OH oscillators of $H_2O$ in the first coordination sphere acted independently and that the rate of non-radiative deexcitation was directly proportional to the number of OH oscillators. Also it was assumed the rate of energy transfer to oscillators outside the first coordination sphere was negligible. When $D_2O$ was substituted for $H_2O$ the non-radiative deexcitation channel was significantly decreased and it was assumed that $D_2O$ molecules contributed to much

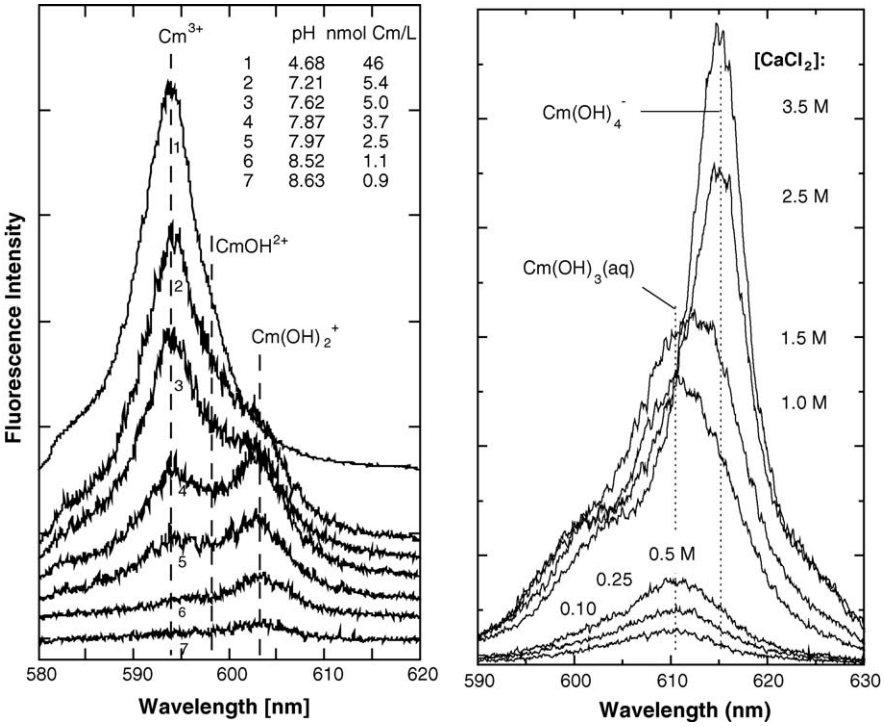


Fig. 6. Emission spectra of the aquo ion and of hydrolysed Cm(III). Left: the emission peak of the Cm(III)(aq) (spectrum 1 at pH 4.68) is red-shifted with increased pH indicating the formation of $CmOH^{2+}$ and $Cm(OH)_2^+$ [44]. Right: at pHc 11.7 the spectra of $Cm(OH)_3$(aq) and $Cm(OH)_4^-$ emerge with increasing $CaCl_2$ concentration, due to the strong ion-interaction between $Ca^{2+}$ and $OH^-$ or $Cm(OH)_x$ compared to $Na^+$ (see text) [45].

lesser extent to the non-radiative relaxation as the O–D vibrations are too low in energy to act as an efficient relaxation path for the Eu(III) ion. Thus the observed rate constant $k_{obs}$ may be written as:

$$k_{obs} = k_{nat} + k_{nonrad} + k_{H_2O}\chi_{H_2O} + k_{D_2O}(1 - \chi_{H_2O}) \quad (22)$$

where $k_{nat}$ is the true radiative rate constant, which is defined as $1/\tau_R$ and can be calculated as described earlier from the Judd–Ofelt theory and intensity measurements. $k_{nonrad}$ is the rate constant for the non-radiative rate processes that do not involve the first water coordination sphere, $k_{H_2O}$ the rate constant proportional to the number of $H_2O$ molecules contained in the first coordination sphere of the Eu(III) ion and $\chi_{H_2O}$ is the mole fraction of $H_2O$ in $H_2O$–$D_2O$ mixtures. The last term $[k_{D_2O}(1 - \chi_{H_2O})]$ in Eq. (22) has been added to the original equation as given by Horrocks and Sudnick [26] to take into account mixtures of $H_2O$ and $D_2O$. Although Horrocks and Sudnick argued that $k_{D_2O}$ is negligibly small, this assumption is not necessary. For further details see Liu and Beitz [25].

Thus if one measures the Eu(III) lifetime in pure $H_2O$ solutions ($\chi_{H_2O} = 1$) and then in pure $D_2O$ solutions ($\chi_{H_2O} = 0$) the difference in the values of $k_{obs}$ will be proportional to the number of $H_2O$ molecules in the first coordination sphere. Addition of complexing agents to the aqueous solutions allowed the determination of the number of $H_2O$ molecules in the complexed Eu(III) species. The method has been estimated to give the coordination number $q$ of the $H_2O$ molecules in the first coordination sphere with an uncertainty of $q = \pm 0.5$ [26]. Recently, Supkowski and Horrocks improved the accuracy of the determination of $q$ to $\pm 0.1$ by a careful recalibration of the experimental data and by introducing terms for the interaction with bulk water and with alcohol O–H and amine N–H oscillators [27].

Beitz [28] studied the fluorescent lifetimes of Cm(III) in aqueous solution to which had been added a number of complexing agents. He determined the number of $H_2O$ molecules in the first coordination sphere of the complexed Cm(III) ion species using the formalism of Horrocks and Sudnick [26] and the Cm(III) lifetime data of Beitz and Hessler [2] as the endpoints. Kimura and Choppin [29], following Horricks and Sudnick methods, measured the Cm(III) lifetimes as a function of the mole fraction of $H_2O$ in dilute perchloric acid $H_2O$–$D_2O$ solutions. Based on the assumption of 9-fold $H_2O$ coordination in the first coordination sphere and neglecting contributions by higher coordination shells, they derived the following equation from their data for room temperature measurements:

$$k_{obs}(Cm(III)) = 14.7\chi_{H_2O} + 0.786 \quad (23)$$

with a correlation coefficient of 0.9999. This equation gives the values of the lifetimes of Cm(III) in pure $H_2O$ and pure $D_2O$ as $64.6 \pm 0.7$ and $1270 \pm 20$ μs. In order to calibrate the number of $H_2O$ molecules in dilute acid solution Kimura and Choppin [29] measured the lifetimes of both the Eu(III) ion and the Cm(III) ion diluted into five lanthanum compounds with known numbers of $H_2O$ molecules in the first coordination sphere. Their Eu(III) data agreed with earlier reported measurements. They derived the empirical relation for the hydration number $q$, the number of $H_2O$ molecules in the first coordination shell:

$$q = 0.65k_{obs}(Cm(III)) - 0.88 \quad (24)$$

with a correlation coefficient of 0.9938 and an estimated uncertainty of $q = \pm 0.5$. Compared to the approach by Horrocks and Sudnick [26], Kimura and Choppin used a simplified method following Barthelemy and Choppin [30]. The decay rate in $D_2O$ was considered to be small compared with that in $H_2O$ and independent of the Cm(III) species, and may therefore be included as a constant, which is fitted to the experimental data. This simplified the determination of hydration numbers considerably, especially for pH titrations for which it is not straightforward to perform parallel experiments in $D_2O$ matching pH and pD. However, in the presence of other quenching processes, e.g. metal to ligand charge transfer, the resulting hydration numbers may be totally wrong.

In an earlier noteworthy review by Billard [31] the applicability of emission decay rates to derive hydration numbers for lanthanides and actinides has been critically discussed. Billard considers non-radiative decay as a not sufficiently understood multi-parametric process and suggests its dependency cannot be dominated by a single parameter such as the hydration number. However, we believe that for selected fluorescent ions with the appropriate experimental conditions, the approach described above is valid. The data presented in this review on Cm(III) clearly show a strong dependency of the decay rate with the hydration number. Obviously, applications to unusual systems such as non-aqueous solutions, the presence of low lying ligand or charge transfer bands, or concentration quenching of precipitated Cm(III) necessitates a thorough inspection of the system. Also more experimental and theoretical work will be needed to fully exploit the potential of this method to determine the hydration number at the trace level concentration range. Keeping in mind all the possible problems, we consider for these reasons the calibration done by Kimura and Choppin [29] as the best available and we use Eq. (24) to calculate hydration numbers.

Lindqvist-Reis et al. [24] reported lifetime measurements for two crystals doped with Cm(III) at low levels with 9 and 8 $H_2O$ molecules each in the first coordination sphere, $[La(H_2O)_9]Cl_3 \cdot 15\text{-crown-}5 \cdot H_2O$ and $[Y(H_2O)_8]Cl_3 \cdot 15\text{-crown-}5$. At 20 °C these two Cm(III) doped crystals had Cm(III) lifetimes of $74 \pm 2$ μs for the crystal with 9 coordinated $H_2O$ molecules and $68 \pm 2$ μs for the crystal with 8 coordinated $H_2O$ molecules. Although the difference in the measured lifetimes is small the molecule with the smaller number of $H_2O$ molecules appears to have the shorter lifetime. The authors suggest that this may be due to the fact that the Cm–O bond length is shorter in the octahydrate and thus energy transfer to the $H_2O$ molecules is more efficient.

### 4.3. Coordination of the Cm(III)(aq)

It is well-established that the inner sphere hydration numbers (i.e. coordination number) for the early and the late trivalent lanthanide aquo ions are 9 and 8, respectively [32]. However, detailed knowledge of the structure and dynamic properties of the aquo ions in the middle of the lanthanide series is lacking. A similar trend is expected for the trivalent actinide aquo ions, although the transition between 9- and 8-coordination may occur later in this series due to the larger ionic radius of the $5f^N$ ion compared to the $4f^N$ ions with same value of $N$, the number of f electrons. Previously, the An(III) hydration numbers have been estimated by interpolation using the values obtained for Ln(III) ions with similar ionic radii [32]. From those results the hydration number for Cm(III) was estimated to be 8.9, for the heavier ions, Bk(III), Cf(III) and Es(III), 8.7, 8.2 and 8.0, respectively, while the lighter ions, Ac(III)–Am(III), were all found to be 9-coordinate. More recently, extended X-ray absorption fine structure (EXAFS) has been used to derive hydration numbers and bond distances for the U(III)–Cf(III) aquo ions. The results, compiled by David and Vokhim [33], showed a steady decrease in the An–O bond distance with increasing atomic number, while the reported hydration numbers were somewhat scattered between about 7 and 10.

Lindqvist-Reis et al. [24] observed a red shift of the emission spectrum of Cm(III) in 0.1 M $HClO_4$ from 593.8 to 595.5 nm by increasing the solution temperature from 20 to 200 °C. By peak deconvolution they deduced an equilibrium between two species with emission maxima at 593.8 and 597.3 nm, which were assigned to 9- and 8-fold hydrated Cm(III)(aq), respectively. The fraction of $Cm(III)(H_2O)_9$ was ~90% at 20 °C and ~60% at 200 °C. The temperature dependence of the intensity ratios followed the Van't Hoff equation with $\Delta H = 13.1 \pm 0.4\ \text{kJ mol}^{-1}$ and $\Delta S = 25.4 \pm 1.2\ \text{J mol}^{-1}\ \text{K}^{-1}$, yielding $\Delta G^{298} = 5.5 \pm 0.6\ \text{kJ mol}^{-1}$. For the purpose of comparison they studied the emission from two crystals doped with Cm(III) at low levels $[La(H_2O)_9]Cl_3 \cdot 15\text{-crown-}5 \cdot H_2O$ and $[Y(H_2O)_8]Cl_3 \cdot 15\text{-crown-}5$. These molecules had 9 and 8 $H_2O$ molecules in the first coordination sphere, respectively. The Cm(III) emission maxima in these crystals at room temperature were at 593.5 and 597.3 nm for the 9- and 8-fold coordination, respectively, in accord with the corresponding aqueous species.

## 5. TRLFS as a speciation tool for Cm(III) in aqueous systems

Speciation, which means the characterisation and quantification of the different Cm(III) species present in solution or at the solid/solution interface, is of great importance in the framework of nuclear waste disposal. Among the ligands present in groundwater that could complex trivalent actinide ions are hydroxide, carbonate and organic materials. Minerals involved in deep geological sites are clay, oxide, silicate, phosphate, etc. Information may be obtained from solutions as well as at solid/solution interfaces about the number of sites, local symmetry, hydration number, ligand exchange rate, and sorption mechanism from the fluorescence line shape, decay rate, and comparison of these spectroscopic characteristics with reference samples.

The sensitivity of TRLFS for Cm(III) is extremely high. Experimentally the limit of detection has been determined by Wimmer and Kim [34] in 0.1 M $HClO_4$ to be $5.5 \times 10^{-12}$ mol/L (signal to noise ratio = 1). In 0.1 M $DClO_4$ the sensitivity is higher by a factor of 14, corresponding to $2.5 \times 10^7$ Cm atoms in the illuminated volume. To derive speciation information a concentration of about $10^{-9}$ to $10^{-7}$ mol/L is necessary. Similar

conditions are valid also for sorption samples of Cm(III), where speciation may be derived at concentrations well below a monolayer (see Section 7.1 below) [35].

The selectivity of TRLFS to distinguish between various Cm(III) complexes is reasonably good. In aqueous solution inorganic and organic Cm-complexes are red-shifted compared to the Cm(III)(aq) up to 14 nm (~400 $cm^{-1}$), which is on the order of the FWHM. For comparison, the emission spectra of lanthanides, such as Eu(III) and Tb(III), show in aqueous solution much smaller shifts and only changes in band shapes and intensities on complexation. Only the weak $^5D_0 \rightarrow {}^7F_0$ transition of Eu(III) shows good selectivity and has been used for speciation, however, with limited sensitivity [36].

It should be noted that TRLFS does not probe the thermodynamic and structural properties of the Cm(III) ground state but those of the first excited state above the ground multiplet, which is about 2 eV higher. The 4f-electron shell of the lanthanides is well shielded by the outer filled 5s, 5p electron shells and does not participate in bonding. To a lesser extent this is also true for the 5f shell of the trivalent actinides with shielding from the filled 6s, 6p shells. No conclusive experimental or theoretical evidence has been given of any differences in thermodynamic or major structural properties between the ground and excited states of a trivalent $f^N$ configuration so far. It seems reasonable therefore to neglect the influence of excitation.

The TRLFS properties of mixtures of different aqueous Cm(III) species depend on the equilibration time between the various species compared to their lifetime. For slow equilibration times, each individual Cm(III) species will decay at its respective lifetime and multiexponential decay is observed. When the equilibration time is fast compared to the lifetimes, a mono-exponential decay is found. The observed decay rate is an average over the decay rates $k_i$ of the individual species $i$ weighted by their molar fraction $\chi_i$:

$$k_{obs} = \sum k_i \chi_i \tag{25}$$

For intermediate cases (lifetimes comparable to equilibration time), a complex exponential decay is found. For just two species a simple solution exists [37].

Emission spectra are superpositions of individual species. The spectra of the pure species as well as their intensities are obtained by peak deconvolution. The emission intensities, FI, of individual species, normalized with respect to the Cm(III) concentration and applied total laser energy, are proportional to absorptivity and lifetime. A separation into these two factors is not possible at trace concentrations because independent information from absorption spectra is not available. The FI factors are necessary in order to derive Cm(III) species concentrations in a mixture.

Processes that may reduce the Cm(III) fluorescence intensity include energy transfer to low lying levels of other ions (Fe(III), Nd(III), etc.) or ligands (triplet states of aromatic compounds or ligand-to-metal-charge-transfer bands). Sensitized fluorescence due to energy transfer from the excited ligand to the Cm(III) (Förster mechanism [38]) may enhance the Cm(III) fluorescence intensity strongly but not the lifetime. This sensitized fluorescence can provide information on the coordination of Cm with aromatic ligands such as humics.

Another important aspect is the precipitation or surface sorption of Cm(III). In $10^{-6}$ M solution the mean distances between Cm(III) ions are about 100 nm, much larger than the Förster distance. If these ions are sorbed onto surfaces or form solid phases, the distance may shrink to less than 1 nm. Exciton migration and trapping also may occur; thus the emission may be partly or completely quenched. The exciton trapping concentration may be much lower than the Cm(III) concentration, which is already very low, and affect the lifetimes. There are some indications that this mechanism may occur. The fluorescence of $Cm(OH)_3$ precipitated in NaOH solution is completely quenched [39,40], contrary to solid $Eu(OH)_3$ [41].

## 6. Complexation reactions

Quantification of Cm(III) fluorescence in aquatic systems permits the determination of thermodynamic data (activity coefficients and equilibrium constants) for hydrolysis and complexation reactions of the dissolved Cm(III) species under the prevailing conditions. If the ligands form sparingly soluble phases, such as hydroxide, fluoride, phosphate, carbonate or silicate, or if the complexation is weak compared to the hydrolysis reaction, the concentration of the complex species will be low also. Near the solubility limit of solid phases, polynuclear and colloidal species may disturb the speciation. Direct speciation by TRLFS of Cm(III) at trace level concentrations has been shown to provide in general more reliable results than solid/water equilibrium reactions or liquid/liquid extraction of, e.g. Am(III) [42]. The following discussion is focussed on complexation studies, where the spectroscopic information has been determined at various ligand concentrations and the Cm(III) emission spectra of pure complex species have been derived.

The spectroscopic characteristics of the Cm(III) complex species with inorganic ligands are listed in Table 6. The complexation constants $\beta^0_{x,y}$, are defined according to the reaction of Cm(III)(aq) with $x$ ligands L:

$$Cm^{3+} + xL^{n-} + yOH^- \Leftrightarrow CmL_x(OH)_y{}^{3-nx-y} \tag{26}$$

and values for inorganic complexes are included in Table 6. For purposes of comparison values extrapolated to zero ionic strength are given.

### 6.1. Hydrolysis

Hydrolysis is the most elementary complexation reaction and starts for Cm(III) around pH 6. Because of sorption of hydrolysed Cm(III), colloid formation, and possible $CO_2$ contamination it is also one of the most difficult reactions to be studied. Wimmer et al. [43] studied the hydrolysis of Cm(III) in the pH-range from 6 to 10 in 0.1 M $NaClO_4$. In addition to the Cm(III) aquo ion, they identified two other species by peak deconvolution of the pH-dependent emission spectra, with fluorescent peaks at 598.8 and 603.5 nm. Based on the intensity ratios of the emission of the individual species they were

Table 6
TRLFS characterization of individual inorganic Cm(III) complexes

| Complex species | $x$ | $\log \beta_x^0$[a] | $\lambda_{max}$ (emis) (FWHM)[b] (nm) | Lifetime (μs) | $q$[c] ±0.5 $H_2O$ | Reference |
|---|---|---|---|---|---|---|
| $Cm(H_2O)_x^{3+}$ | 9 | | 593.8 (6.7) | 64 ± 3 | (9.0) | [24] |
| | 8 | −0.95 ± 0.01 | 597.3 (10) | – | (8.0) | |
| $Cm(OH)_x^{3-x}$ | 1 | 6.8 ± 0.5* | 598.8 (11) | 76 ± 2 | 8.1 | [43,44] |
| | 2 | 12.9 ± 0.7* | 603.5 (11) | 80 ± 10 | 7.2 | |
| | 3 | 15.8 ± 0.5* | 610.3 | 117 ± 5 | 4.7 | [45] |
| | 4 | 0.6 ± 0.3[d] | 614.8 | 33 ± 2 | (–) | |
| $CmF^{2+}$ | | 3.44 ± 0.05 | 601.3 (8.5) | 65 ± 3 | 9.1 | [59] |
| $CmCl_x^{3-x}$ | 1 | 0.24 ± 0.03 | 594.9 | | | [47,49] |
| | 2 | −0.74 ± 0.05 | 598.3 | 80 | 7.2 | |
| $Cm(SO_4)_x^{3-2x}$ | 1 | 3.28 ± 0.03* | 596.2 (9.5) | 88 ± 2 | 6.5 | [58] |
| | 2 | 3.59 ± 0.03* | 599.5 (8.0) | 95 ± 8 | 6.0 | |
| | 3 | – | 602.2 (5.5) | 195 ± 3 | 2.5 | |
| $CmH_2PO_4^{2+}$ | | 2.62 ± 0.03 | 599.9 (8.6) | – | | [60] |
| | | | 600.7 (10) | 95 | 5.9 | [61] |
| $Cm(CO_3)_x^{2-2x}$ | 1 | 8.10 ± 0.3 | 598.5 (7.4) | 79 | 7.3 | [53,55] |
| | 2 | 13.0 ± 0.6 | 603.0 (7.3) | 89 | 6.4 | |
| | 3 | 15.2 ± 0.4 | 605.7 (6.8) | 126 | 4.3 | |
| | 4 | 13.0 ± 0.5 | 607.5 (8.2) | 256 | 1.6 | |
| $CmHCO_3^{2+}$ | | 3.1 ± 0.3* | 594.9 (8.0) | 70 | 8.4 | [54] |
| $CmSiO(OH)_3^{2+}$ | | 7.74 ± 0.08 | 598.5 (11.9) | 85 ± 2.5 | 6.7 | [62] |

[a] Complex stability constant, extrapolated to zero ionic strength, superscript asterisk (*) denotes $\log \beta_x^0$ taken from the OECD-NEA-Thermodynamic Data Base update report [42].
[b] $\lambda_{max}$, wavelength of the emission maximum; FWHM, full-width at half maximum.
[c] Number of water molecules in the first coordination sphere, calculated from lifetime by Eq. (24).
[d] Stepwise equilibrium constant $\log K_4^0$ ($Cm(OH)_3(aq) + OH^- \Leftrightarrow Cm(OH)_4^-$); SIT coefficient $\Delta\varepsilon = -0.58\,kg\,mol^{-1}$ in $CaCl_2$ medium).

able to assign the species to $Cm(OH)^{2+}$ and $Cm(OH)_2^+$ and to derive stability constants. Fanghänel et al. [44] studied Cm(III) hydrolysis in NaCl aqueous media varying the NaCl concentration between 0.01 and 6.15 mol/kg $H_2O$ (molal scale). The emission spectra in 2 m NaCl are shown in Fig. 6 (left side) as a function of pH. They deduced similar emission spectra for the complexes $Cm(OH)^{2+}$, $Cm(OH)_2^+$ as Wimmer et al. [43]. However, the contribution of the $Cm(OH)^{2+}$ species to the emission spectra was found to be much weaker than in $NaClO_4$ solution. The Cm(III) speciation was determined as a function of NaCl concentration. All emission spectra could be deconvoluted with the same three species, indicating that even at 6.15 molal NaCl concentrations, complexation with $Cl^-$ is not significant (see Section 6.2.1).

Mono-exponential decay was observed by Wimmer et al. [43] over the experimental pH-range. At pH 6.93 a lifetime of 72 ± 2 μs was measured, which was assigned to the lifetime of $Cm(OH)^{2+}$. Taking into account an equilibrium of 65% Cm(III)(aq) and 35% $Cm(OH)^{2+}$, a lifetime of 76 ± 2 μs is determined from Eq. (25) for $Cm(OH)^{2+}$. A lifetime of 80 ± 10 μs was measured at pH 9.84 and should correspond to $Cm(OH)_2^+$, which is the dominant species (95%) at this pH. However, due to the low Cm(III) concentration this value has a large uncertainty. No quench rate for a $OH^-$ group coordinated directly to Cm(III) has been reported. If we use the quench rate of half that of $H_2O$, as proposed by Supkoswki and Horrocks for Eu(III) [27] and assume a total coordination number of 9, the calculated lifetimes for these two Cm(III) hydroxide species are 69.3 and 73.2 μs, which are shorter that the experimental values.

Above pH 11 the neutral solution species $Cm(OH)_3(aq)$ is expected to dominate the speciation [42]. However, due to the low solubility of Cm(III) in this pH range ($10^{-11}$ mol/L) it could not be detected by TRLFS. Also no evidence was found for the formation of the anionic $Cm(OH)_4^-$ species in NaOH solution up to 7.5 M [40]. However, recent findings by Rabung et al. showed that the formation of the neutral and anionic complexes is strongly enhanced in the presence of $CaCl_2$ and simultaneously the sorption of Cm(III) is decreased [45]. The reason for this behavior is the strong ion interaction between $OH^-$ and hydroxo complexes with $Ca^{2+}$ compared to the interaction with $Na^+$ or $K^+$. In accordance with solubility measurements on $Nd(OH)_3(s)$ they identified $Cm(OH)_3(aq)$ and $Cm(OH)_4^-$ in alkaline 0.1–3.5 M $CaCl_2$ solutions (Fig. 6, right side).

### 6.2. Inorganic ligands

#### 6.2.1. $Cl^-$ complexation

Contrary to other speciation methods, TRLFS of Cm(III) in aqueous solution is sensitive only to inner sphere complexation. Outer sphere complexes show nearly identical spectra as Cm(III)(aq). This is in accord with the species concept used in the thermodynamic approach for concentrated brine solutions [46]. So called outer sphere complexes are not treated as defined species, but as an effect of the electrolyte medium on the activity

coefficient. Using the Pitzer model for inner sphere complex species, the ionic strength dependency of the complexation constants can be quantified in highly concentrated electrolytes.

Fanghänel et al. [47] have studied the $Cl^-$ complexation of Cm(III) in the range of 0–20 molal $Cl^-$ concentration at acidic pH. No changes in the emission spectra or lifetimes have been observed compared to the Cm(III)(aq) up to 4 m $Cl^-$ concentration. At higher $Cl^-$ concentrations two new emission peaks at 594.9 and 598.3 nm appeared, which were assigned to $CmCl^{2+}$ and $CmCl_2^+$. In supersaturated $Cl^-$ solution (20.4 m) a further band appeared at 603 nm that is possibly $CmCl_3$(aq). From 4.5 to 12 m $Cl^-$ concentration conditional stability constants were derived for the first and second chloro complexes by peak deconvolution. In a 5.6 m $CaCl_2$ solution a lifetime of 80 μs was found corresponding to a hydration number of 7.2. From the Cm(III) speciation in this solution an average coordination number for $Cl^-$ of 1.2 was calculated, which is consistent with the hydration number of 7.2. The results also are consistent with the EXAFS analysis of Cm(III) in LiCl [48]. In 8.7 M LiCl, which has a comparable water activity as 5.6 m $CaCl_2$, Allen et al. found 1.2 coordinated $Cl^-$ atoms. Note that both methods, TRLFS and EXAFS, indicated that the total coordination number remained constant at ∼9 at higher $Cl^-$ concentrations. The difficulty in deriving thermodynamic data for this weakly complexing ligand is that the constant ionic strength concept cannot be used because no experimental data below 4 molal $Cl^-$ concentrations are available. This situation necessitates simultaneous fitting of stability constants and Pitzer parameters [49].

### 6.2.2. Carbonate complexation

Carbonate is ubiquitous in any groundwater and forms strong complexes with actinides. Therefore, the first exploratory TRLFS studies on Cm(III) complexation dealt with carbonate as a ligand, especially in strong carbonate solution [28,50,51]. Kim et al. [52] characterized and quantified by TRLFS the monocarbonato complex $Cm(CO_3)^+$. The complexes $Cm(CO_3)_x^{3-2x}$ ($x = 2$, 3) were characterized by TRLFS under the assumption that the latter is the limiting complex. Later Fänghänel et al. [53] deduced the tetracarbonato as the limiting complex. In this comprehensive study, they varied the carbonate concentrations over six orders of magnitude by adjusting the pH at given $CO_2$ partial pressure (open system) and by batch experiments with various ratios of $HCO_3^-/CO_3^{2-}$ (closed system). The complexes $Cm(CO_3)_x^{3-2x}$ ($x = 1$–4) were characterized and quantified by TRLFS in 0.1 m $NaCl^-$ solution. Furthermore they showed the existence of a bicarbonate complex $CmHCO_3^{2+}$ that dominated at pH 5.5 at $CO_2$ partial pressures above 1 bar [54]. They also found that the Cm(III) carbonate complexation depended only on the $CO_3^{2-}$ concentration but not on pH, excluding the presence of significant amounts of the ternary complex $Cm(OH)CO_3$. The emission spectra of the pure complex species derived by peak deconvolution are shown at the top of Fig. 7. The Cm(III) carbonate speciation was quantified by TRLFS in the range from 0 to 6 m NaCl solutions for the parameterization of the Pitzer ion-interaction model [55]. The species distribution derived in 1 m NaCl is shown at the bottom of Fig. 7 as a function of the carbonate concentration. In this work, the

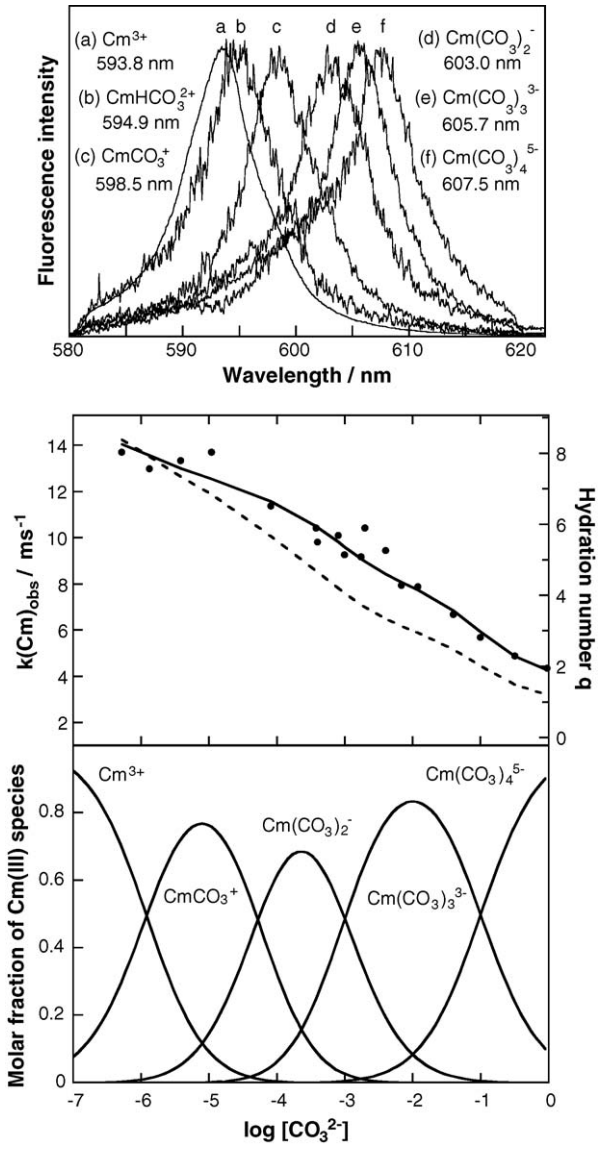


Fig. 7. Cm(III) complexation in carbonate solution [55]. Top: emission spectra of pure Cm(III) complex species in carbonate medium. Bottom: the Cm(III)-carbonate derived species distribution in 1 m NaCl solution is show as a function of the carbonate concentration in the lowest graph. The abscissa, log $[CO_3^{2-}]$ is the same for both the middle and lowest graphs. Middle: this graph shows the decay rates (left scale) and hydration numbers (right scale) as a function of the carbonate concentration. Dots indicate experimental data. The dashed line is calculated assuming bidentate carbonate binding and a total coordination number of 9, the solid line is a fit of individual decay rates for all Cm(III) species according to Eq. (25) using the mole fractions of the carbonate species as shown in the bottom figure. The derived individual lifetimes are listed in Table 6.

emission spectra for the Cm(III) carbonato species derived from dilute NaCl solutions were representative of the Cm(III) complex species in strong brine solution, indicating that the TRLFS of the Cm(III) species is sensitive primarily to the first coordination sphere, and is not much affected by cations and anions in the outer sphere.

Mono-exponential decay was found in all Cm-carbonate solutions, indicating fast equilibria of the complexation reactions. The measured lifetimes are shown in the middle part of

Fig. 7 together with a fit of the individual lifetimes of the complex species according to Eq. (25) (solid line). The individual lifetimes recalculated from the original data are listed together with other spectroscopic data in Table 6.

Recently, Vercouter et al. [56] investigated the carbonate complexation of Cm(III) at high ionic strength (3 M $NaClO_4$) in the temperature range 10–70 °C. Although the experimental fluorescence spectra obtained for the Cm(III) carbonato species were similar to those obtained by Fanghänel et al. [53] for carbonate concentrations that range over three orders of magnitude, the lower value obtained for the formation constant of $Cm(CO_3)_3^{3-}$ ($\log K_3^0 = 0.88 \pm 0.05$) is due to the interpretation considering a limiting tricarbonato complex of Cm(III) similar to the analyses of solubility measurements of Am(III) and its counterpart lanthanide Eu(III) [57]. The stepwise formation constant for the tricarbonato complex $Cm(CO_3)_3^{3-}$ was determined as a function of temperature and was found to vary linearly with $1/T$ as also observed from solubility data for Am(III) in 4 M NaCl. The thermodynamic data were extrapolated to $I = 0$ with the SIT formula ($\Delta H_3^0$ (298 K) = 9.4 ± 4.8 kJ $mol^{-1}$ and $\Delta S_3^0$ (298 K) = 48 ± 23 J $mol^{-1}$ $K^{-1}$).

### 6.2.3. Other inorganic complexes

Further systematic studies on the complexation of Cm(III) with sulfate [58], fluoride [59], dihydrogen phosphate [60,61] and silicate [62] have been performed with the aim of characterizing the Cm(III) complex species by TRLFS and deriving thermodynamic data. The results, which are not discussed in detail in this review, are summarized in Table 6. Cm(III) complexation with nitric acid to concentrations of 16 M has been studied by various authors, however, without identification of the complex species present [28,63,64]. Studies on the interaction of Cm(III) with various iso and hetero-polyoxoanions, such as $W_{10}O_{36}^{12-}$, $P_2W_{17}O_{61}^{10-}$ and $SiW_{11}O_{39}^{8-}$ have been reviewed by Yusov and Shilov [65].

## 6.3. Organic ligands

### 6.3.1. Polyamino acids

The results of preliminary studies performed on the complexation of Cm(III) with *trans*-1,2-diaminocyclohexanetetraacetic acid (CDTA), diethylenetriaminepentaacetic acid (DTPA) [28] and ethylenediaminetetraacetic acid (EDTA) [51] are summarized in Table 7. Kimura and Choppin [29] reported the hydration numbers of Cm(III) and Eu(III) complexes of EDTA, DTPA, CDTA, nitrilotriacetic acid (NTA), triethylenetetraaminehexaacetic acid (TTHA) and hydroxyethylenediamine-triacetic acid (HEDTA) in aqueous solution at particular pH values. They noted the residual hydration number for the Cm(III) ion in these systems was consistently larger than that found for the Eu(III) analogue. In all the systems they measured the total coordination number in the first coordination sphere, defined as the sum of the number of ligand donor groups plus the number of coordinated $H_2O$ molecules, was 8.8 ± 0.5 for Eu(III) and 9.3 ± 0.4 for Cm(III) (omitting their data for the NTA complex). They cautiously concluded that "the total coordination number for Cm(III) is possibly 0.5 larger than that of Eu(III) in polyaminopolycarboxylate complexes". Curiously, the measured lifetimes for CDTA by Beitz [28] (66 μs in $H_2O$ and 115 μs in $D_2O$) and Kimura and Choppin [29] (139 μs in $H_2O$) are completely contradictory. It appears that a quenching contamination led to wrong results for the lifetime measurements by Beitz [28] in $H_2O$ and also in $D_2O$, but must have cancelled out in the determination of the hydration number. Therefore, the hydration number $q = 3.8$ calculated by Kimura and Choppin using Eq. (24) agrees with that of Beitz (see Table 7).

Wang et al. [40] have investigated the complexation of Cm(III) with HEDTA, EDTA, NTA and oxalic acid focussing on highly alkaline solutions up to 7.5 M NaOH. The complexation with HEDTA was discussed in detail. The emission spectra of Cm(III) with 0.01 M HEDTA in 0.1 M NaOH solution showed two peaks at 600.4 and 607.0 nm with bi-exponential decay indicating a slow ligand exchange reaction (lifetimes of 227 and 456 μs). These species were assigned to the complexes $Cm(HEDTA)(H_2O)_2$ and non-hydrated $Cm(HEDTA)_2^{3-}$, respectively. In 0.5–7.5 M NaOH solution an additional emission band centered at 616.0 nm appeared. The short lifetime of 82 μs, corresponding formally to a hydration number of 7.1, did not seem consistent with the observed strong red shift of the emission band. Therefore the authors favored another deactivation pathway; the chelation of colloidal Cm(III)-bearing nanoparticles with HEDTA. Such colloids might be formed from impurities present in strong NaOH solutions and easily sorb hydrolysed Cm(III) species. The emission spectrum of Cm(III) in 0.5 M NaOH and 0.01 M HEDTA is shown in Fig. 8 together with the spectra of the three discussed species derived by peak deconvolution.

### 6.3.2. Cm α-hydroxy-acetate

The fluorescence spectroscopic properties of the Cm(III) and Eu(III) complexes with α-hydroxy-acetate (glycolate) have been studied by Stumpf et al. [66]. In 1 M glycolate solution three complex species of Cm(III) have been identified and quantified in the pH range from 4.5 to 11.7. Based on the pH dependent speciation and on the lifetimes, the following assignments have been deduced. The first complex is identified as $Cm(HOCH_2COO)_4^-$; above pH 8.7 a coordinated $H_2O$ is deprotonated, and at pH 10.5 a chelate complex, $CmOH(HOCH_2COO)_3(OCH_2COO)_4^{2-}$ or $Cm(HOCH_2COO)_2(OCH_2COO)_2^{2-}$, is formed. The bi-exponential decay at pH 10.6 indicated a slow closure of the chelate ring. The reverse reaction occurred after more than 1 day when the solution was acidified to pH 4.7. For the Eu(III) system, the first and second complexes could not be differentiated by TRLFS. Furthermore, the Eu(III) complex is much more labile compared to the Cm(III) case.

### 6.3.3. Humic substances and model ligands

Natural organic matter, such as humic and fulvic acids, found in many groundwaters or as coatings of minerals, exhibits strong interactions with actinides. Due to the poorly defined composition and structure of these macromolecules the kinds of interaction with metal ions and its quantification are still controversial. A number of studies on the interaction of Cm(III) with

Table 7
TRLFS characterization of individual organic Cm(III) complexes

| Ligand[a] | Ligand concentration/pH | $\lambda_{max}$ (emis) (FWHM)[b] (nm) | Lifetime (μs) | $q$[c] ±0.5 $H_2O$ | Reference |
|---|---|---|---|---|---|
| EDTA | $10^{-3}$ M/pH 3 | 603.8 (4) | 126 | 4.4 | [51] |
| | $5.7 \times 10^{-6}$ M/pH 4.6 | – | 141 ± 1 | 3.7 | [29] |
| | $10^{-2}$ M/pH 6–13 | 599.4 | 234 | 1.9 | [40] |
| | $10^{-2}$ M/[$OH^-$] = 0.5 M | 609.1 | 347 | 1.0 | |
| | $10^{-2}$ M/[$OH^-$] = 7.5 M | 616.6 | 95 | (5.9) | |
| DTPA | 0.1 M/near-neutral pH | 607 | 271 ± 8<br>764 ± 23[d] | 1.5<br>1.5[e] | [28] |
| | $5.7 \times 10^{-6}$ M/pH 4.6 | – | 257 ± 1 | 1.7 | [29] |
| CDTA | 0.1 M/near-neutral pH | 604 | 66 ± 2<br>115 ± 3[d] | 9.1<br>3.8[e] | [28] |
| | $5.7 \times 10^{-6}$ M/pH 4.6 | – | 139 ± 4 | 3.8 | [29] |
| NTA | $5.7 \times 10^{-6}$ M/pH 4.6 | – | 91 ± 2 | 6.3 | |
| | $10^{-2}$ M/pH 6–13 | 596.4 | 220 | 2.1 | [40] |
| | $10^{-2}$ M/[$OH^-$] = 0.5 M | 606.1 | 336 | 1.1 | |
| | $10^{-2}$ M/[$OH^-$] = 7.5 M | 613.2 | 66 | (9.0) | |
| TTHA | $5.7 \times 10^{-6}$ M/pH 4.6 | – | 444 ± 4 | 0.6 | [29] |
| HEDTA | $5.7 \times 10^{-6}$ M/pH 4.6 | – | 129 ± 2 | 4.2 | |
| | $10^{-2}$ M/pH 6–13 | 600.4 | 227 | 2.0 | [40] |
| | $10^{-2}$ M/[$OH^-$] = 0.5 M | 607.0 | 456 | 0.3 | |
| | $10^{-2}$ M/[$OH^-$] = 7.5 M | 616.0 | 82 | (7.1) | |
| Glycolic acid | 1 M/pH 4.4–8.7 | 602.3 | 206 ± 3 | 2.3 | [66] |
| | 1 M/pH 8.7–10.3 | 605.6 | 206 ± 3 | 2.3 | |
| | 1 M/pH 10.3–11.7 | 611.3 | 295 ± 15 | 1.3 | |
| 5-Sulfo-salicylic acid | 0.05–0.1 M/pH 6.2–6.55 | 597.8 (10.5)<br>604.5 (9.0) | –<br>– | –<br>– | [71,72] |
| Phthalic acid | $10^{-3}$ M/pH 6.0 | 597.7 (8.0) | 91 ± 2 | 6.3 | [72] |
| Humic acid | 60–7600 μg/L pH 6.0 | 601.0 (11) | 72 ± 5 (80%)<br>145 (20%) | 3.3[e] for slow component | [34,69,72] |
| | Deuterated solution | 601.0 (11) | 200 (64%)[d]<br>603 (36%)[d] | | |
| Fulvic acid | 40–2500 μg/L pH 6.0 | 600.3 (12) | 70 ± 5 (80%)<br>142 (20%) | – | [34,70,72] |

[a] For full names of the ligands see text.
[b] $\lambda_{max}$, wavelength of the emission maximum; FWHM, full-width at half maximum.
[c] Number of water molecules in the first coordination sphere, calculated from lifetime by Eq. (24), brackets indicate that the authors considered the values doubtful because of other quench processes.
[d] Lifetime measured in $D_2O$.
[e] Calculated by the Horrocks equation $q = 0.63 \times (k_{H_2O} - k_{D_2O})$ calibrated by Beitz [28].

humic and fulvic acids and model ligands have addressed to this question.

Moulin et al. [67,68] studied the interaction of Cm(III) with humic and fulvic acid by TRLFS. Using an excitation wavelength at 337 nm, they observed an emission maximum at 600 nm with a strongly increased intensity compared to the Cm(III)aq. Based on this sensitized emission they measured the intensity as a function of humate/fulvate concentration and derived from this fluorescence titration the complexing capacity and stability constant. Kim et al. and Buckau et al. investigated the complexation of Cm(III) with purified and well characterized humic acid [34,69] and fulvic acid [34,70], both isolated from the Gorleben aquifer (Germany), at pH 6.0 in 0.1 M $NaClO_4$. The excitation spectrum of Cm humate at pH 6 is shown in Fig. 9 and compared with that of Cm(III) in the absence of humate in the range from 370 to 405 nm. The 5f excitation bands are significantly broadened upon humate complexation compared to Cm(III)aq. Furthermore, the excitation spectrum of the Cm(III) humate complex is superimposed on the background of humate/fulvate absorption. This ligand absorption results in ligand to metal energy transfer. As a consequence of this indirect excitation the emission spectra of Cm(III) humate and fulvate complexes show an increase in intensity of 1.47 and 6.11 in comparison with the Cm(III)aq (see Fig. 10).

In addition to the Cm(III)aq species, the authors identified and characterized humate/fulvate complex species which were quantified at various ligand concentrations. A problem for the thermodynamic quantification is caused by the unknown

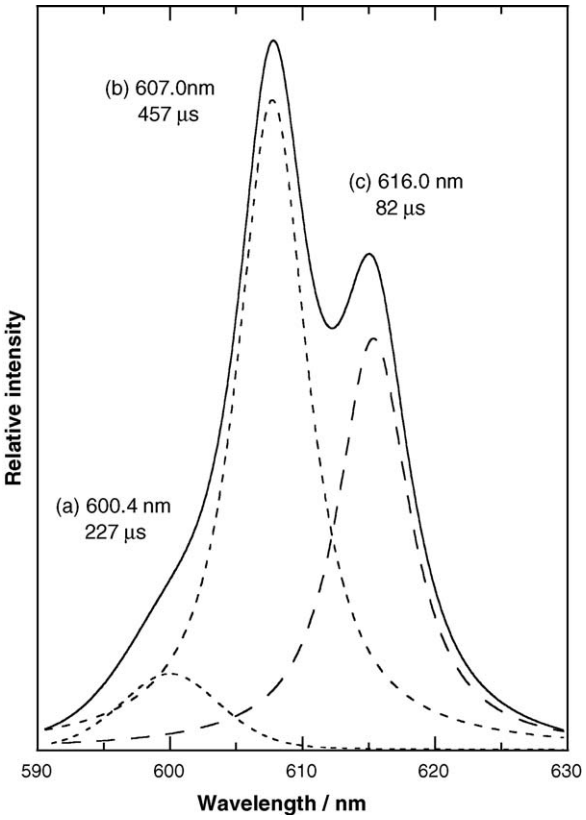


Fig. 8. Emission spectra of Cm(III) in 0.5 M NaOH and 0.01 HEDTA and of the deconvoluted components of (a) Cm(HEDTA), (b) $Cm(HEDTA)_2^{3-}$ and (c) another Cm HEDTA species probably sorbed to $Cm(OH)_3$ colloids. This redrawing was done only on the fit of the mixed spectra, but not on the noisy experimental spectrum [40].

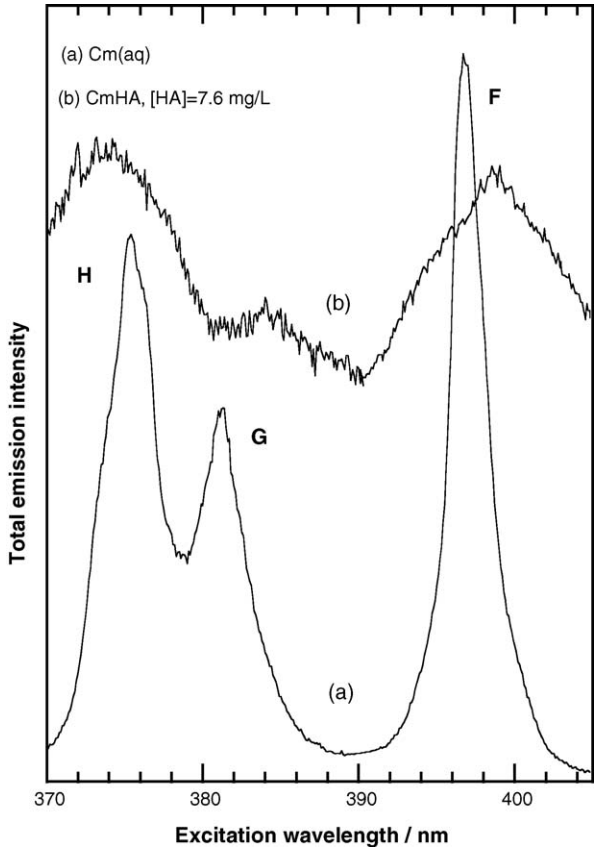


Fig. 9. Excitation spectra of the Cm(III) emission (integrated from 580 to 620 nm) of (a) Cm(III)(aq) and (b) the Cm(III) complex with humic acid (Gohy-573). The latter shows direct excitation of Cm(III) broadened bands compared to Cm(III)(aq) and sensitized emission due to energy transfer from the excited ligand to the Cm(III) [34,69].

ligand concentration. It was found that only a part of the proton exchanging functional groups of the humate/fulvate were accessible to complexation with metal ions. Therefore an operational parameter, the loading capacity LC, was introduced, which was determined from the saturation metal concentration. For Am(III), the LC was determined at pH 6 in 0.1 M $NaClO_4$ to be 0.622 and 0.649 for humic and fulvic acids, respectively. The resulting stability constants were found to be independent of metal concentration and pH.

The emission of the pure Cm(III) humate and fulvate complex species followed a bi-exponential decay in $H_2O$ and also in $D_2O$. The lifetime of the slow component corresponded to a hydration number of 3.3, which is consistent with the coordination of three bidentate complexing groups. The fast component could be due to energy transfer to low lying ligand or charge transfer states. Unfortunately, the photodynamics of the humate/fulve entity itself is not sufficiently understood. The energy transfer from the humate/fulvate system to Cm(III) was compared by Panak et al. [71,72] with model complexes with aromatic complexing ligands, such as phthalic and 5-sulfosalicylic acid. This study found that the observed energy transfer in the natural organic ligands was consistent with the presence of aromatic benzene rings in conjugation with the coordinating functional group, such as 2-hydroxo benzoic acid.

Above pH 6 the Cm(III) emission of the humate complex was red-shifted, indicating the formation of other complex species. This effect was analyzed by Panak et al. [73] in a natural groundwater from Gorleben and by Morgenstern et al. [74] with the purified humic acid, isolated from the same groundwater. These authors demonstrated the presence of Cm(III) ternary hydroxo-humate complexes, which may dominate the speciation in the neutral pH-range under natural conditions. TRLFS of Cm(III) has been used also to study the interactions in the ternary system actinide ion, mineral surface and humic/polyacrylic acid [75–77].

## 7. Interaction of Cm(III) with mineral phases

The reaction of actinides with the mineral surface provides retardation and retention mechanisms for actinide migration in the geosphere. The understanding of the processes on a molecular level is imperative for a sound quantitative description and for the long-term prediction of actinide migration in the geosphere. TRLFS on Cm(III) has been used to identify various sorption mechanisms, such as ion exchange, specific adsorption or incorporation into the bulk mineral phase. This identification is primarily based on the hydration number derived from

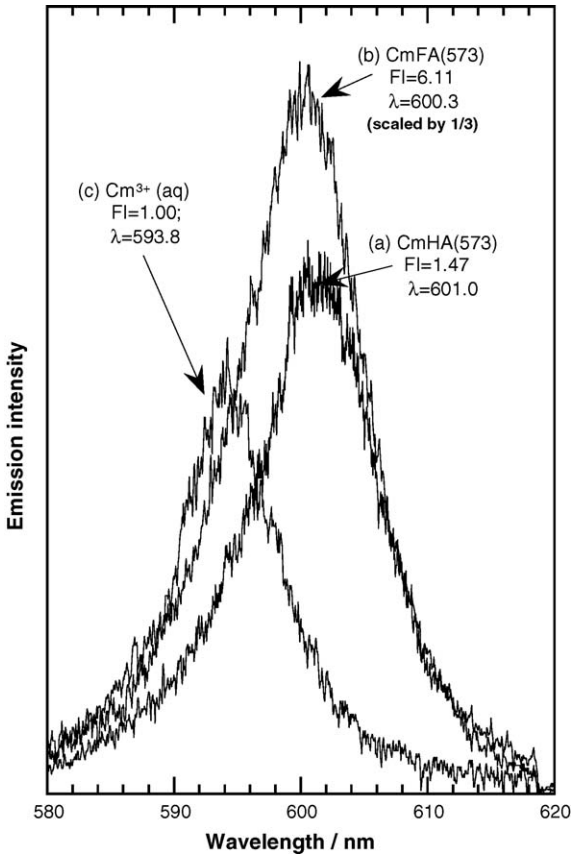


Fig. 10. Emission spectra of Cm(III) complexed to humic and fulvic acids in comparison to the Cm(III)(aq) [34,72].

the lifetime. As seen in Fig. 11 the hydration numbers vary greatly depending on specific adsorption ($q \approx 5$) or incorporation ($q \approx 0$). For ion exchange in the clay interlayer (outer sphere complexation) the lifetime and emission spectrum corresponds to that of the Cm(III)aq ($q \approx 9$).

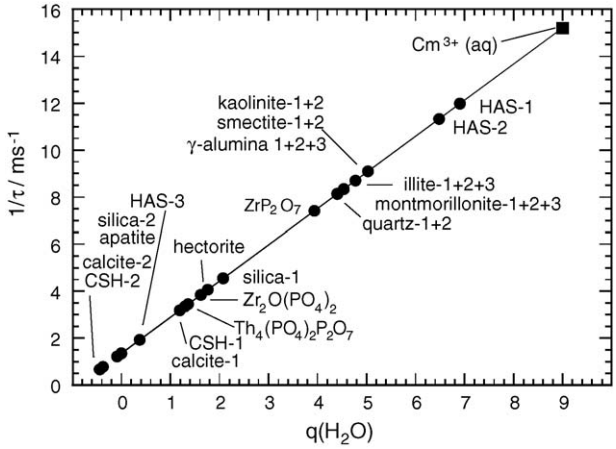


Fig. 11. Experimental decay rates of Cm(III) interacting with various mineral phases and correlated hydration numbers according to Eq. (24). Notice the clustering of purely adsorbed Cm(III) around $q = 5$ and of incorporated Cm(III) with $q = 0$. Mineral names, abbreviations of species and numbering follow Tables 8 and 9.

In the following sections, interface and incorporation reactions are discussed separately. However, in some cases the adsorption reaction is followed by an incorporation reaction and these two mechanisms cannot be separated. The spectroscopic results are summarized in Tables 8 and 9.

### 7.1. Interface reactions

Interface reactions of Cm(III) with oxides, such as alumina, silica, clay and phosphate minerals have been studied by TRLFS and are discussed below. TRLFS on Cm(III) has been used to identify and quantify the species sorbed onto the surface of minerals because of its high sensitivity (fraction of a monolayer) and good selectivity. This technique is particularly crucial not only to validate speciation calculations but also to elucidate the sorption mechanism.

#### 7.1.1. Sorption onto alumina

Stumpf et al. [78] have characterized and quantified the surface complexes of Cm(III) onto colloidal pyrogenic γ-alumina by TRLFS based on a previous sorption study of Am(III) and Eu(III) by Rabung et al. [79]. Two Cm(III) surface complexes emitting at 601.2 and 603.3 nm have been identified in the pH range from 4 to 10. In a later extension of this study (to pH 13) a third surface species emitting at 605.7 nm was found. The reanalyzed results are summarized in Table 8. The lifetimes for all the surface complexes were ~110 μs corresponding to 5 $H_2O$ or $OH^-$ ligands in the first coordination shell of Cm(III). From these results, inner sphere monodentate Cm(III) complexes bound to surface aluminol groups were assumed. With increasing pH, ternary hydroxo complexes were formed with the neutral end-member ≡AlO-Cm$(OH)_2(H_2O)_3$ above pH 11.8. The distribution of the various sorbed and dissolved Cm(III) species were fitted as a function of pH with a surface complexation model.

In order to validate the applicability of surface complexation models to highly charged actinide ions and to elucidate the influence of site heterogeneity and surface potential, Rabung et al. [35] performed a Cm(III) sorption experiment on single crystals of α-$Al_2O_3$. Sapphire wafers (10 mm × 10 mm × 0.5 mm size) with selected faces (0 0 1, 1 1 0, 0 1 2, 0 1 8 and 1 0 4) were cleaned and characterized by various methods (XPS, AFM and LEED). After floating on the surface of about $10^{-6}$ mol/L Cm(III) solutions at pH 4.5 and 5.1 for 1–2 days a very low Cm(III) surface concentration of 3–43 pmol/cm$^2$ at pH 5.1 was measured by α-spectrometry and autoradiography. Fluorescence results from Cm(III) could be obtained even at this low concentration despite the TRLFS sensitivity being hampered by a Cr(III) impurity, emitting at 694.3 nm, present in the sapphire matrix. As shown in Fig. 11, the spectroscopic properties of the 0 0 1 surface were rather similar to the first sorption species of the γ-alumina system [78], indicating that both phases form similar alteration products in contact with the aqueous phase, such as bayerite (γ-Al$(OH)_3$). The four other faces showed almost identical spectroscopic properties, indicating similar binding sites, but with different surface coverage (see Fig. 12 and Table 8). The Cm(III) sorption onto single faces of α-alumina was enhanced

Table 8
TRLFS characterization of individual Cm(III) species at the mineral/water interface

| Mineral phase | Species | Site density/ loading[a] | pH range[b] | $\lambda_{max}$ (emis) (FWHM)[c] (nm) | Lifetime (μs) | $q$[d] ±0.5 $H_2O$ | Reference |
|---|---|---|---|---|---|---|---|
| Silica (pyrogenic $SiO_2$) | 1 | 2.3/(<0.6%) | 6.2–7.3 | 602.3 (8) | 220 ± 14 | 2.1 | [80] |
| | 2 | | >7.3 (8.7) | 604.9 (13.2) | 740 ± 35 | 0 | |
| Quartz (cryst. $SiO_2$) | 1 | | 5.3–6.0 | 601.4 | 123 ± 10 | 4.4 | [82] |
| | 2 | | >6.0 (9.0) | 603.6 | 123 ± 10 | 4.4 | |
| γ-Alumina (pyrogenic γ-$Al_2O_3$) | 1 | 1.0/(0.23%) | 5.2–6.6 | 600.6 (8.3) | 110 ± 7 | 5.0 | [78] |
| | 2 | | 6.6–11.5 | 602.5 (10.5) | 110 ± 7 | 5.0 | |
| | 3 | | >11.5 (13.2) | 605.7 (9.5) | 110 ± 7 | 5.0 | [e] |
| α-Alumina[f] (single cryst. α-$Al_2O_3$) (*h k l*)→ | (0 0 1) | (1.9%)[f] | 4.5 and 5.1 | 601.3 (10.6) | 107 ± 1 | 5.2 | [35] |
| | (0 1 2) | (0.42%) | 4.5 and 5.1 | 603.2 (10.5) | 162 ± 3 | 3.1 | |
| | (1 1 0) | (0.29%) | 4.5 and 5.1 | 603.5 (10.5) | 192 ± 3 | 2.5 | |
| | (1 0 4) | (0.18%) | 4.5 and 5.1 | 603.8 (10.5) | 185 ± 3 | 2.6 | |
| | (0 1 8) | (0.18%) | 4.5 and 5.1 | 603.6 (10.5) | 158 ± 3 | 3.2 | |
| Kaolinite | 1 | | 5.7–6.4 | 598.3 | 110 ± 7 | 5.0 | [83] |
| | 2 | | >6.4 (8.3) | 603.3 | 110 ± 7 | 5.0 | |
| Smectite | 1 | | 6.1–6.4 | 598.3 | 110 ± 7 | 5.0 | |
| | 2 | | >6.4 (8.3) | 603.3 | 110 ± 7 | 5.0 | |
| Montmorillonite (Ca-loaded) | 1 | | 4–6 | 599.1 (10.0) | 120 ± 15 | 4.5 | [84,85] |
| | 2 | | 6.5–8 | 603.2 (9.0) | 120 ± 15 | | |
| | 3 | | 8–11.8 | 607.1 (18.5) | 120 ± 15 | | |
| | 4 | | > 11.8 (12.3) | 620.0 (7.7) | 753 ± 88 | 0 | |
| Illite | 1 | –/(1.19%) | 4.8–6.7 | 598.8 (12.5) | 115 ± 4 | 4.8 | |
| | 2 | | 6.7–10.7 | 602.3 (13.6) | 115 ± 4 | 4.8 | |
| | 3 | | > 10.7 (12) | 605.5 (20.0) | 115 ± 4 | 4.8 | |
| $Th_4(PO_4)P_2O_7$ | 1 | | 4 | 606.7(11) | 290 ± 10 | 1.4 | [61] |
| $ZrP_2O_7$ | 1 | | 4.4 | 602.8(9.5) | 135 ± 10 | 3.9 | |
| $Zr_2O(PO_4)_2$ | 1 | | 3.7 | 605.0 (9) | 260 ± 10 | 1.6 | |

[a] Given are the site density (atoms/$nm^2$) and its max. loading by Cm(III) (in %).
[b] pH-range, where the given species plays a dominant role. (pH) indicates highest measured pH.
[c] $\lambda_{max}$, wavelength of the emission maximum; FWHM, full-width at half maximum.
[d] Number of water molecules in the first coordination sphere, calculated from lifetime by Eq. (24).
[e] Unpublished results by Ref. [78].
[f] For α-$Al_2O_3$ single crystals the (*h k l*) indices are listed, loading is given for pH 5.1.

Table 9
TRLFS characterization of individual Cm(III) species incorporated into mineral phases

| Mineral phase | Species | pH range | $\lambda_{max}$ (emis) (FWHM)[a] (nm) | Lifetime (μs) | $q$[b] ± 0.5 $H_2O$ | Reference |
|---|---|---|---|---|---|---|
| Apatite $Ca_{10}(PO_4)_6F_2$ | | 5.8 | 609.1 (3) | 820 ± 20 | 0 | [61] |
| Calcite ($CaCO_3$) | 1 | – | 607.5 (10) | 314 ± 6 | 1.2 | [88] |
| | 2 | – | 618.0 (10) | 1302 ± 75 | 0 | |
| Aluminosilicate (HAS) | 1 | 4–5 | 598.5 (7.5) | 83.5 ± 3.7 | 6.9 | [81,90] |
| | 2 | 5–6 | 601.8 (12.2) | 88.3 ± 5.2 | 6.5 | |
| | 3 | >6 | 606.8 (14.8) | 518 ± 25 | 0.4 | |
| Ca-silicate hydrate (CSH) | 1 | 13.3 | 618.9 | 289 ± 11 | 1.4 | [39] |
| | 2 | 13.3 | 620.9 | 1482 ± 200 | 0 | |
| Portlandite ($Ca(OH)_2$) | | 13.5 | 613.6 (10) | 62 ± 8 | (9.6) | [86] |
| Powellite ($CaMoO_4$) | | 5.5 | 611.0 (8.6) | 165 | (3.1) | [87] |
| Hectorite (synthetic) | | 10 | 609.3 | 246 | 1.8 | [97] |

[a] $\lambda_{max}$, wavelength of the emission maximum; FWHM, full-width at half maximum.
[b] Number of water molecules in the first coordination sphere, calculated from lifetime by Eq. (24); brackets indicates that the authors considered the values doubtful because of other quench processes.

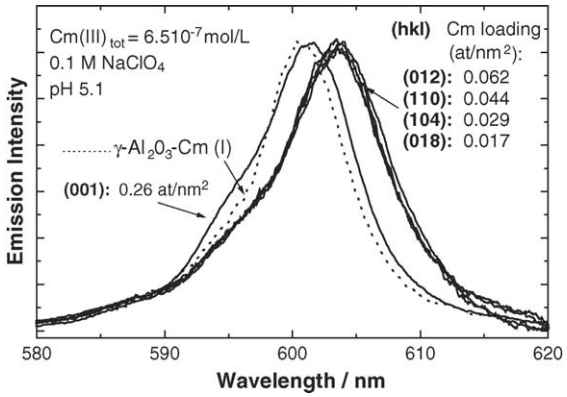


Fig. 12. Emission spectra of Cm(III) sorbed onto single crystal faces of α-$Al_2O_3$ (sapphire wafers) in comparison with γ-$Al_2O_3$, normalized to the same peak height. Cm(III) surface concentrations (in atoms/nm$^2$) were measured by α-spectrometry [35].

by 2–3 orders of magnitude at pH 4.5 compared to the results for the γ-alumina study. This increase possibly can be ascribed to a shift in the point of zero charge to lower pH values in the case of single crystals. This initial TRLFS study on α-alumina single crystals is presently being complemented by the application of a variety of other spectroscopic and microscopic methods (XAFS, XPS, AFM and non-linear vibrational spectroscopy) as well as with quantum mechanical calculations.

### 7.1.2. Sorption onto silica

Contrary to the formation of inner sphere surface complexes in alumina systems, Chung et al. [80] found a different sorption mechanism for the interaction of Cm(III) with amorphous pyrogenic silica colloids. Two Cm(III) species, emitting at 602.3 and 604.9 nm were identified in the pH range from 5 to 9 with lifetimes of 220 and 740 μs, respectively. According to Eq. (24) this corresponds to two and zero coordinated water molecules in the first coordination sphere of these two complexes compared with five water molecules generally found for surface complexes such as in alumina systems. It was rationalised that the second species represents non-hydrated Cm(III) incorporated into the bulk silica structure or to a ternary surface complex with orthosilicic acid, which is known to be formed by dissolution of amorphous silica in millimolar concentrations. The same species were observed by Kim et al. [81] by neutralisation of $1.3 \times 10^{-2}$ M alkaline silicate in the presence of Cm(III). To understand the role of silicic acid on the incorporation process of Cm(III) in the silica structure, Stumpf [82] studied the sorption of Cm(III) onto synthetic quartz by TRLFS. Again two complex species were identified, however, with lifetimes of 123 μs, corresponding to a hydration number of 4.4. Obviously, due to the lower solubility of quartz compared to amorphous silica, the concentration of orthosilicic acid was too low to cause the Cm(III) to incorporate in the silica bulk structure or to form silicate complexes at the surface.

### 7.1.3. Sorption onto clay minerals

The sorption behavior onto various clay minerals is more complex when compared to the simple mineral phases discussed so far. As has been demonstrated in several publications, TRLFS provides the possibility to distinguish clearly between various sorption mechanisms. Stumpf et al. [83] studied the sorption of Cm(III) in suspensions of purified and well characterized kaolinite and smectite in 0.025 M $NaClO_4$ in the pH range from 3.7 to 8.3. They deduced from the pH-dependent emission spectra the presence of two species with nearly identical spectra for both minerals (see Table 8). The lifetimes were found to be equal for both species sorbed onto kaolinite and smectite and also identical to that in the γ-alumina system ($110 \pm 7$ μs), corresponding to a hydration number of 5.0. Furthermore, the emission spectra of both species were similar to the corresponding species in the γ-alumina system but not with the silica system. The authors concluded that the Cm(III) is bound to octahedral coordinated aluminium at the edges of the clay particles. Below pH 5 the Cm(III)(aq) fraction is higher than 90% in both the kaolinite and smectite system. However, the cation exchange capacity was determined to be larger by a factor of 20 for smectite than for kaolinite in the acidic range due to intercalation of metal ions in the interlayers of smectite, which are not present in kaolinite. It was concluded that Cm(III) in the interlayers keeps its complete hydration sphere. Thus the ion exchange mechanism within the interlayers of swelling clay minerals is easily distinguished from inner sphere complexation with the adsorption sites.

The sorption of Cm(III) onto illite and montmorillonite has been studied recently in parallel to an extensive wet-chemistry sorption study on Eu(III) [84]. To prevent interference by ion exchange at the montmorillonite interlayers these sites were loaded with Ca(II) by working in 0.066 $Ca(ClO_4)_2$ solution. In addition to the two species found for the kaolinite and smectite systems (see above), at pH > 8 a third species was deduced, emitting at 605.5 and 607.1 nm in the illite and montmorillonite systems, respectively. The emission spectra of all three complexes compare well with those in the γ-alumina system. Again the lifetime of the sorbed Cm(III) does not vary with pH. The lifetimes are $115 \pm 4$ and $120 \pm 15$ μs, corresponding to hydration numbers of 4.8 and 4.5 for the illite and montmorillonite system, respectively. At pH 12 a sudden shift of the emission maximum and an increase of the lifetime to $753 \pm 88$ μs was observed for the $Ca^{2+}$ loaded montmorillonite. The similarity to the emission spectrum of Cm(III) incorporated in Ca-silicate hydrate (CSH), studied by Tits et al. [39] was taken as evidence for the formation of such a mixed alteration phase from the Ca-rich montmorillonite. It was possible to model both the pH-dependent sorption of Cm(III) and the isotherms and pH-dependent sorption of Eu(III) with the same set of SCM parameters. Weak and strong sorption sites, which described the non-ideal sorption isotherms, were assumed to be the sites which determined the spectral properties of the bound Cm(III) [85].

### 7.1.4. Sorption onto phosphate phases

The sorption of Cm(III) onto phosphate minerals is complex because of the possibility of several active sorption sites, and the resulting variation in the fluorescence spectra (linewidth, peak energies and lifetimes) by comparison with reference samples can give structural information. Cavellec et al. [61] studied the sorption behavior of Cm(III) onto $Th_4(PO_4)_4P_2O_7$ (TDP) and

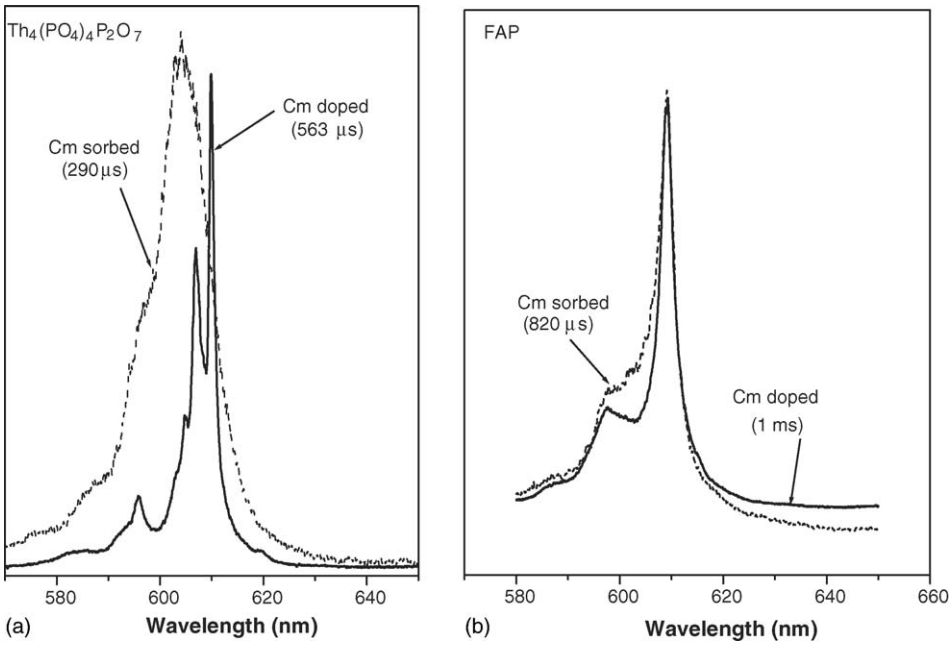


Fig. 13. Emission spectra of Cm(III) adsorbed on and incorporated in (a) thorium phosphate diphosphate and (b) fluoroapatite (FAP) [61].

compared these data with other phosphate reference materials, $ZrP_2O_7$ and $Zr_2O(PO_4)_2$, using TRLFS.

By comparison of the line shapes of the emission spectra and the lifetimes of Cm(III) species sorbed and doped on (into) $Th_4(PO_4)_4P_2O_7$, Cavellec et al. [61] showed that it was possible to identify the sorption mechanism (Fig. 13a). In the doped sample, Cm(III) ions replaced the Th(IV) ions and two major distinct sites were determined using selective excitation with two intense peaks at 604.8 and 609 nm, and a shoulder corresponding to a third minor site due to charge compensation. The temperature dependence of the lines clearly demonstrated that the first band at 597 nm can be attributed to transitions from the highest energy component of the $^6D_{7/2}$ excited multiplet to the $^8S_{7/2}$ ground state. The emission band of the sorbed sample exhibited only one broad band with FWHM of 11 nm showing a different environment. A short lifetime with mono-exponential decay was measured for the sorbed sample (290 μs compared to 563 and 610 μs for the two sites of the doped samples) indicated the formation of only one surface complex bound to the solid. Comparison with reference samples was performed in order to elucidate the active site. The similarity of the fluorescence lifetimes and the peak maxima between Cm(III) sorbed onto $Th_4(PO_4)_4P_2O_7$ ($\tau = 290$ μs, $\lambda_{max} = 606.7$ nm) and Cm sorbed onto $Zr_2O(PO_4)_2$ ($\tau = 260$ μs, $\lambda_{max} = 605$ nm) indicated that Cm(III) was preferentially bound to a $PO_4^-$ site rather than a $P_2O_7$ site since the lifetime of $ZrP_2O_7$ emission is much shorter ($\tau = 135$ μs).

### 7.2. Incorporation into secondary phases

The formation of secondary solid phases is considered to be one of the key processes for the immobilization of radionuclides in the environment. The mechanisms by which a radionuclide is incorporated into a mineral are of fundamental importance and at present, not well understood. Questions to be addressed include: Which metal ions of the surface or solid may be replaced, e.g. by Cm(III)? How many different sites are present which may coordinate with Cm(III)? How is the charge compensated in the case of heterovalent substitution? Is the formation of solid solutions kinetically or thermodynamically controlled? TRLFS of Cm(III) doped into dielectric host matrices, as reviewed in the first part of this work may provide useful information to elucidate the formation of solid solutions. In the following, the discussion is focussed on the incorporation of Cm(III) into apatite, calcite, aluminosilicate and calcium silicate hydrates. Furthermore, the incorporation of Cm(III) in cement systems has been studied by Stumpf et al. [86], as has the incorporation of Cm(III) in powellite ($CaMoO_4$), a secondary phase generated by dissolution of highly active waste borosilicate-glass, by Bosbach et al. [87]. Pieper et al. [97] studied the synthesis of hectorite in the presence of Cm(III). The results of these studies are summarized in Table 9.

#### 7.2.1. Apatite

Apatites are extremely stable geologic materials that have a great capacity for the retention of heavy metal and actinide ions. Heavy metal ions such as Pb(II), Sr(II), Cd(II) and so forth are immobilized by substitution for Ca(II) after diffusion through the apatite channels if the impurity cation ionic radius is close to that of Ca(II) (0.99 Å). By comparison of the line shapes of the emission spectra and the lifetime of Cm(III) sorbed at pH 5.8 and doped on (in) the fluoroapatite $Ca_{10}(PO_4)_6F_2$, Cavellec et al. [61] were able to demonstrate that Cm(III) is incorporated into the lattice. The linewidth is very narrow, ~3 nm, with a peak maximum at 609.1 nm, close to that obtained from the doped standards (Fig. 13b). Moreover, the lifetime (820 μs) of sorbed Cm(III) fluoroapatite is similar to those for the doped standards (1 ms). This is in contrast to other phosphate minerals

discussed before for which fluorescence linewidths were usually ~9–11 nm. The incorporation of Cm(III) into the apatite can be due either to sorption via a diffusion mechanism through the channels to substitute for Ca(II) by ion exchange or formation of a secondary phase generated after dissolution of soluble apatite.

#### 7.2.2. Calcite

Stumpf et al. [88] have studied the interaction of Cm(III) in calcite suspensions at various contact times between 24 h and 6 months. The spectra associated with calcite could be deconvoluted into two spectral components, emitting at 607.5 (complex 1) and 618.0 nm (complex 2). The spectrum of complex 1 was very similar to the spectrum of the carbonate solution complex $Cm(CO_3)_4^{5-}$ (see Fig. 7, top), however, by centrifugation it was proven that this species is associated with calcite. The extraordinary red shift of the second Cm species indicated an extreme change of the ligand field of the Cm(III). With longer contact time the emission intensity of the Cm/calcite complex 1 decreased and the intensity of complex 2 increased. The emission decay of Cm(III) in calcite showed bi-exponential behavior, indicating the presence of two sites. Two different lifetimes of the Cm(III) species were found: $314 \pm 6$ and $1302 \pm 75$ μs, corresponding to a hydration number of 1.2 and 0 for complex 1 and complex 2, respectively. Complex 2 was assigned to Cm(III) substituting for an octahedrally coordinated Ca(II), whereas complex 1 replaced a Ca(II) at the surface and is coordinated by one $H_2O$ molecule.

#### 7.2.3. Hydroxyaluminosilicates

The formation of aluminosilicate colloids under simulated natural conditions has been studied in the presence of trivalent actinides by Kim et al. and Panak et al. [81,89,90]. In these studies colloidal hydroxyaluminosilicates were prepared by co-precipitation of acidic Al(III) and alkaline silicate solution in the presence of Cm(III) under various conditions. The amounts of colloids, their average size, and their stability were determined by Laser-induced Breakdown Detection (LIBD) as a function of pH. The Cm(III) interaction with the hydroxyaluminosilicate was characterized by TRLFS. Two complexes with peak maxima at 598.5 nm (Cm-HAS(I)) and 601.8 nm (Cm-HAS(II)) in the pH region from 4 to 9 were observed. Using oversaturated silicate solution (0.02 mol/L), containing more reactive oligomeric silicates, a further Cm(III) species with a peak maximum of 606.8 nm (Cm-HAS(III)) was formed even in the absence of Al. Lifetime measurements of Cm-HAS(III) have shown that the Cm(III) loses its primary hydration sphere and is imbedded into the structure of the hydroxyaluminosilicate colloids.

#### 7.2.4. Calcium silicate hydrates

Tits et al. [39] studied the uptake of trivalent f-elements by calcium silicate hydrates (CSH phases) at pH 13.3 in batch-type sorption experiments for Eu(III) and complemented this work with a TRLFS study on Cm(III) for selected samples. A strong uptake of Cm(III) with fast sorption kinetics and linear isotherms was found. At the beginning of the sorption experiment no emission of Cm(III) was detected. However, with increasing equilibration time, an emission band appeared at about 620 nm, which was still increasing after 119 d. TRLFS revealed that the 620 nm emission consisted of two components with emission maxima at 618.9 nm ($\tau = 289 \pm 11$ μs) and 620.9 nm ($\tau = 1482 \pm 200$ μs), corresponding to hydration numbers of 1.4 and 0, respectively, suggesting that both species are incorporated into the CSH structure. Based on the structure of tobermorite, they assigned the first Cm(III)-species to the replacement of either an octahedrally coordinated "stable Ca" or of the 7-fold coordinated "labile" Ca in the interlayers between the Ca-silicate sheets, which are coordinated by one and two water molecules, respectively [91]. The second non-hydrated Cm(III)-species was assigned as substituting for 7-fold oxygen coordination site originating from Si tetrahedra.

Further experiments to elucidate the mechanism of the slow increase of the emission intensity with time showed that Cm(III) was present in the solution as a non-fluorescent species and not sorbed to the cuvette walls. The same behavior was found in 0.1 M NaOH solution in the absence of CSH. This indicated that non-fluorescent Cm(III) is present in solution as colloidal $Cm(OH)_3(s)$. With increasing time the Cm hydroxide phase will be dissolved and the released Cm(III) will be incorporated into the CSH phase. The total quenching of the emission is not necessarily an intrinsic property of the Cm(III) hydroxide, it could be also due to trapping impurities at concentration substantial lower than that of Cm(III). For Cm(III) co-precipitated in 1 M NaOH with an excess of $5.2 \times 10^{-4}$ M Gd(III) an emission maximum at 607.1 nm and a lifetime of $56 \pm 2$ μs was reported by Tits et al. [39].

## Acknowledgments

This work was supported in part by the Director, Office of Science, Office of Basic Energy Sciences, of the U.S. Department of Energy under Contract No. DE-AC02-05CH11231.

## References

[1] N.M. Edelstein, J. Alloys Compd. 223 (1995) 197.
[2] J.V. Beitz, J.P. Hessler, Nucl. Technol. 51 (1980) 169.
[3] W.T. Carnall, H. Crosswhite, H.M. Crosswhite, J.P. Hessler, N. Edelstein, J.G. Conway, G. Shalimoff, J. Chem. Phys. 72 (1980) 5089.
[4] W.T. Carnall, J. Chem. Phys. 96 (1992) 8713.
[5] B.G. Wybourne, Spectroscopic Properties of Rare Earths, Interscience, New York, 1965.
[6] F. Auzel, O.L. Malta, J. Phys. 44 (1983) 201.
[7] R.D. Cowan, The Theory of Atomic Structure and Spectra, University of California Press, Berkeley, 1981.
[8] C. Görller-Walrand, K. Binnemans, Spectral intensities of f–f transitions, in: K.A. Gschneidner Jr., L. Eyring (Eds.), Handbook on the Physics and Chemistry of Rare Earths, vol. 25, Elsevier, Amsterdam, 1998, p. 101.
[9] W.T. Carnall, K. Rajnak, J. Chem. Phys. 63 (1975) 3510.
[10] B.R. Judd, Phys. Rev. 127 (1962) 750.
[11] G.S. Ofelt, J. Chem. Phys. 37 (1962) 511.
[12] J.D. Axe Jr., Phys. Rev. 136 (1964) A42.
[13] M. Illemassene, K.M. Murdoch, N. Edelstein, J.C. Krupa, J. Lumin. 75 (1997) 77.
[14] G.K. Liu, J.V. Beitz, J. Huang, J. Chem. Phys. 99 (1993) 3304.
[15] M. Illemassene, N. Edelstein, K.M. Murdoch, M. Karbowiak, R. Cavellec, S. Hubert, J. Lumin. 86 (2000) 45.

[16] K.M. Murdoch, N.M. Edelstein, L.A. Boatner, M.M. Abraham, J. Chem. Phys. 105 (1996) 2539.
[17] P. Thouvenot, S. Hubert, N. Edelstein, Phys. Rev. B 50 (1994) 9715.
[18] K.M. Murdoch, R. Cavellec, E. Simoni, M. Karbowiak, S. Hubert, M. Illemassene, N.M. Edelstein, J. Chem. Phys. 108 (1998) 6353.
[19] N. Edelstein, W. Easley, J. Chem. Phys. 48 (1968) 2110.
[20] Y.A. Barbanel', Radiochim. Acta 78 (1997) 91.
[21] L.J. Nugent, P.G. Laubereau, G.K. Werner, K.L. Vander Sluis, J. Organomet. Chem. 27 (1971) 365.
[22] R.G. Gutmacher, E.K. Hulet, J.G. Conway, J. Opt. Soc. Am. 54 (1964) 1403.
[23] T. Kimura, R. Nagaishi, Y. Kato, Z. Yoshida, Radiochim. Acta 89 (2001) 125.
[24] P. Lindqvist-Reis, R. Klenze, G. Schubert, T. Fanghänel, J. Phys. Chem. B 109 (2005) 3077.
[25] G.K. Liu, J.V. Beitz, Optical spectra and electronic structure, in: L.R. Morss, N.M. Edelstein, J. Fuger (Eds.), The Chemistry of the Actinide and Transactinide Elements, Springer, Dordrecht (Chapter 18), 2006.
[26] W.D. Horrocks Jr., D.R. Sudnick, J. Am. Chem. Soc. 101 (1979) 334.
[27] R.M. Supkowski, W.D. Horrocks, Inorg. Chim. Acta 340 (2002) 44.
[28] J.V. Beitz, Radiochim. Acta 52–53 (1991) 35.
[29] T. Kimura, G.R. Choppin, J. Alloys Compd. 213–214 (1994) 313.
[30] P.P. Barthelemy, G.R. Choppin, Inorg. Chem. 28 (1989) 3354.
[31] I. Billard, Lanthanide and actinide solution chemistry as studied by time-resolved emission spectroscopy, in: K.A. Gschneidner Jr., J.-C.G. Bünzli, V.K. Pecharsky (Eds.), Handbook on the Physics and Chemistry of Rare Earths, vol. 33, Elsevier, Amsterdam, 2003, p. 465.
[32] E.N. Rizkalla, G.R. Choppin, Lanthanides and actinides hydration and hydrolysis, in: J. Gschneider, K.A.L. Eyring, G.R. Choppin, G.H. Lander (Eds.), Handbook on the Physics and Chemistry of Rare Earths, vol. 18, Elsevier, Amsterdam, 1994, p. 529.
[33] F.H. David, V. Vokhmin, New J. Chem. 27 (2003) 1627.
[34] H. Wimmer, J.I. Kim, Laser-induzierte optische Spektroskopie zur Spezi-ation von f-Elementen in natürlichen aquatischen Systemen, Report RCM 00992. Institut für Radiochemie, Technische Universität München, Garching, 1992, 234 pp.
[35] T. Rabung, D. Schild, H. Geckeis, R. Klenze, T. Fanghänel, J. Phys. Chem. B 108 (2004) 17160.
[36] P.J. Breen, W.D. Horrocks Jr., Inorg. Chem. 22 (1983) 536.
[37] W.D. Horrocks Jr., V.K. Arkle, F.L. Liotta, D.R. Sudnick, J. Am. Chem. Soc. 105 (1983) 3455.
[38] T. Förster, Discuss. Faraday Soc. 27 (1959) 7.
[39] J. Tits, T. Stumpf, T. Rabung, E. Wieland, T. Fanghänel, Environ. Sci. Technol. 37 (2003) 3568.
[40] Z. Wang, A.R. Felmy, Y.X. Xia, M.J. Mason, Radiochim. Acta 91 (2003) 329.
[41] R.L. Cone, R. Faulhaber, J. Chem. Phys. 55 (1971) 5198.
[42] R. Guillaumont, T. Fanghänel, J. Fuger, I. Grenthe, V. Neck, D.A. Palmer, M.H. Rand, Update on the Chemical Thermodynamics of Uranium, Neptunium, Plutonium, Americium and Technetium, Elsevier, Amsterdam, 2003.
[43] H. Wimmer, R. Klenze, J.I. Kim, Radiochim. Acta 56 (1992) 79.
[44] T. Fanghänel, J.I. Kim, P. Paviet, R. Klenze, W. Hauser, Radiochim. Acta 66–67 (1994) 81.
[45] T. Rabung, M. Altmaier, V. Neck, FZK-INE, unpublished results.
[46] T. Fanghänel, J.I. Kim, J. Alloys Compd. 271 (1998) 728.
[47] T. Fanghänel, J.I. Kim, R. Klenze, Y. Kato, J. Alloys Compd. 225 (1995) 308.
[48] P.G. Allen, J.J. Bucher, D.K. Shuh, N.M. Edelstein, I. Craig, Inorg. Chem. 39 (2000) 595.
[49] T. Könnecke, T. Fanghänel, J.I. Kim, Radiochim. Acta 76 (1997) 131.
[50] P. Decambox, P. Mauchien, C. Moulin, Radiochim. Acta 48 (1989) 23.
[51] R. Klenze, J.I. Kim, H. Wimmer, Radiochim. Acta 52–53 (1991) 97.
[52] J.I. Kim, R. Klenze, H. Wimmer, W. Runde, W. Hauser, J. Alloys Compd. 213–214 (1994) 333.
[53] T. Fanghänel, H.T. Weger, T. Könnecke, V. Neck, P. Paviet-Hartmann, E. Steinle, J.I. Kim, Radiochim. Acta 82 (1998) 47.
[54] T. Fanghänel, H.T. Weger, G. Schubert, J.I. Kim, Radiochim. Acta 82 (1998) 55.
[55] T. Fanghänel, T. Könnecke, H. Weger, P. Paviet-Hartmann, V. Neck, J.I. Kim, J. Solut. Chem. 28 (1999) 447.
[56] T. Vercouter, P. Vitorge, B. Amekraz, E. Giffault, S. Hubert, C. Moulin, Inorg. Chem. 44 (2005) 5833.
[57] T. Vercouter, P. Vitorge, N. Trigoulet, E. Giffaut, C. Moulin, New J. Chem. 29 (2005) 544.
[58] P. Paviet, T. Fanghänel, R. Klenze, J.I. Kim, Radiochim. Acta 74 (1996) 99.
[59] W. Aas, E. Steinle, T. Fanghänel, J.I. Kim, Radiochim. Acta 84 (1999) 85.
[60] A. Morgenstern, J.I. Kim, Humat- und Phosphatkomplexierung von Actinidionen im grundwasserrelevanten pH-Bereich, Report RCM 00797. Institut für Radiochemie, Technische Universität München, Garching, 1997, 172 pp.
[61] R. Cavellec, C. Lucas, E. Simoni, S. Hubert, N. Edelstein, Radiochim. Acta 82 (1998) 221.
[62] P.J. Panak, M.A. Kim, R. Klenze, J.I. Kim, T. Fanghänel, Radiochim. Acta 93 (2005) 133.
[63] T. Kimura, Y. Kato, H. Takeishi, G.R. Choppin, J. Alloys Compd. 271–273 (1998) 719.
[64] D.Y. Chung, E.H. Lee, J.H. Yoo, T. Kimura, J. Nucl. Sci. Technol. Suppl. 3 (2002) 332.
[65] A.B. Yusov, V.P. Shilov, Radiochemistry 41 (1999) 1.
[66] T. Stumpf, T. Fanghänel, I. Grenthe, J. Chem. Soc. Dalton Trans. (2002) 3799.
[67] C. Moulin, P. Decambox, P. Mauchien, V. Moulin, M. Theyssier, Radiochim. Acta 52–53 (1991) 119.
[68] V. Moulin, J. Tits, C. Moulin, P. Decambox, P. Mauchien, O. de Ruty, Radiochim. Acta 58–59 (1992) 121.
[69] J.I. Kim, H. Wimmer, R. Klenze, Radiochim. Acta 54 (1991) 35.
[70] G. Buckau, J.I. Kim, R. Klenze, D.S. Rhee, H. Wimmer, Radiochim. Acta 57 (1992) 105.
[71] R. Klenze, P. Panak, J.I. Kim, J. Alloys Compd. 271 (1998) 746.
[72] P. Panak, R. Klenze, J.I. Kim, H. Wimmer, J. Alloys Compd. 225 (1995) 261.
[73] P. Panak, R. Klenze, J.I. Kim, Radiochim. Acta 74 (1996) 141.
[74] M. Morgenstern, R. Klenze, J.I. Kim, Radiochim. Acta 88 (2000) 7.
[75] Y. Takahashi, T. Kimura, Y. Minai, Geochim. Cosmochim. Acta 66 (2002) 1.
[76] G. Montavon, T. Rabung, H. Geckeis, B. Grambow, Environ. Sci. Technol. 38 (2004) 4312.
[77] X.K. Wang, T. Rabung, H. Geckeis, P.J. Panak, R. Klenze, T. Fanghänel, Radiochim. Acta 92 (2004) 691.
[78] T. Stumpf, T. Rabung, R. Klenze, H. Geckeis, J.I. Kim, J. Colloid Interface Sci. 238 (2001) 219.
[79] T. Rabung, T. Stumpf, H. Geckeis, R. Klenze, J.I. Kim, Radiochim. Acta 88 (2000) 711.
[80] K.H. Chung, R. Klenze, K.K. Park, P. Paviet-Hartmann, J.I. Kim, Radiochim. Acta 82 (1998) 215.
[81] M.A. Kim, P.J. Panak, J.I. Yun, A. Priemyshev, J.I. Kim, Colloids Surf. A: Physicochem. Eng. Aspects 254 (2005) 137.
[82] S. Stumpf, Spektroskopische Untersuchungen zu Sorptionsmechanismen von dreiwertigen Actiniden an Feldspäten, Quarz und Ferrihydrit, Ph.D. Thesis, Ruprechts-Karls-University Heidelberg, Heidelberg, 2004, 161 pp.
[83] T. Stumpf, A. Bauer, F. Coppin, J.I. Kim, Environ. Sci. Technol. 35 (2001) 3691.
[84] T. Rabung, M.C. Pierret, A. Bauer, H. Geckeis, M.H. Bradbury, B. Baeyens, Geochim. Cosmochim. Acta 69 (2005) 5393.
[85] M.H. Bradbury, B. Baeyens, H. Geckeis, T. Rabung, Geochim. Cosmochim. Acta 69 (2005) 5403.
[86] T. Stumpf, J. Tits, C. Walther, E. Wieland, T. Fanghänel, J. Colloid Interface Sci. 276 (2004) 118.
[87] D. Bosbach, T. Rabung, F. Brandt, T. Fanghänel, Radiochim. Acta 92 (2004) 639.

[88] T. Stumpf, T. Fanghänel, J. Colloid Interface Sci. 249 (2002) 119.
[89] M.A. Kim, P.J. Panak, J.I. Yun, J.I. Kim, R. Klenze, K. Köhler, Colloids Surf. A: Physicochem. Eng. Aspects 216 (2003) 97.
[90] P.J. Panak, M.A. Kim, J.I. Yun, J.I. Kim, Colloids Surf. A: Physicochem. Eng. Aspects 227 (2003) 93.
[91] S.A. Hamid, Kristallographica 154 (1981) 189.
[92] G.K. Liu, S.T. Li, V.V. Zhorin, C.-K. Loong, M.M. Abraham, L.A. Boatner, J. Chem. Phys. 109 (1998) 6800.
[93] J. Sytsma, K.M. Murdoch, N.M. Edelstein, L.A. Boatner, M.M. Abraham, Phys. Rev. B 52 (1995) 12668.
[94] P. Thouvenot, Propriétés optiques de Eu, Am, et Cm dans la structure cubique $ThO_2$. Application à l'analyse de traces d'actinides par spectrofluorimétrie laser, Thèse de l'Université Paris Sud, Orsay, 1993.
[95] N.A. Stump, G.M. Murray, G.D. Del Cul, R.G. Haire, J.R. Peterson, Radiochim. Acta 61 (1993) 129.
[96] Y.A. Barbanel', G.P. Chudnovskaya, R.B. Dushin, V.V. Kolin, V.P. Kotlin, S.N. Nekhoroshkov, M.V. Pen'kin, Radiochim. Acta 78 (1997) 69.
[97] H. Pieper, D. Bosbach, P.J. Panak, K. Dardenne, J. Rothe, M.A. Denecke, T. Fanghänel, Geochim. Cosmochim. Acta 68 (2004) A504.